Universidad de Valladolid

UNIVERSIDAD DE VALLADOLID

ESCUELA DE INGENIERIAS INDUSTRIALES

Grado en Ingeniería en Tecnologías Industriales

Particle resolved model of gas-flow inside a pipe with pellet filling

Autor:

Valle Gaisán, Ángel

Eusebio de la Fuente López

Technische Universität Dresden

Valladolid, marzo 2023.

TFG REALIZADO EN PROGRAMA DE INTERCAMBIO

TÍTULO:	Particle resolved model of gas-flow inside a pipe with pellet filling
ALUMNO:	Ángel Valle Gaisán
FECHA:	10/03/2023
CENTRO:	Technische Universität Dresden
UNIVERSIDAD:	Technische Universität Dresden
TUTOR:	Eusebio de la Fuente López

RESUMEN

Algunos métodos prometedores de almacenamiento de hidrogeno basan su funcionamiento en los reactores de lecho fijo. El CFD es una herramienta muy útil en el diseño de dichos reactores, ya que permite realizar precisas predicciones de comportamiento con un bajo coste.
Estas aproximaciones del proceso son muy útiles para determinar el tamaño y forma óptimos del reactor, así como de las partículas de su interior. Sin embargo, el gran esfuerzo computacional que implican los modelos más detallados, hace que este método no sea siempre la opción preferida.
El objetivo de este trabajo es describir el proceso de generación y validación de un modelo computacional PRCFD de un reactor de lecho fijo relleno de partículas esféricas, el estudio de la influencia de algunas de sus características y la comparación de los resultados de pérdida de presión con los de un modelo empírico usando la ecuación de Ergun.

PALABRAS CLAVE

Almacenamiento de hidrógeno, reactores de lecho fijo, Dinámica de Fluidos Computacional, modelo de partícula discreta, esfuerzo computacional.

BACHELOR THESIS

Topic:	Particle resolved model of gas-flow inside a pipe with pellet filling
Editor:	Angel Valle Gaisán
Matriculation number:	5118642
Processing period:	01.10.2022 to 28.02.2023
Place, date of submission:	Dresden, 28.02.2023
Number:	B 08/22
Maintainer:	Dr.-Ing. Andreas Jäger
	Dipl.-Ing. Oscar Baños
Responsible. Professor:	Prof. Dr. Cornelia Breitkopf

Text pages:	63

Task description of Bachelor Thesis for Mr. Angel Valle Gaisan

Thema: Particle resolved model of gas-flow inside a pipe with pellet filling.

The continuous increase of the proportion of renewable energies in the energy supply constitutes the core of the transformation of the energy market of electricity, heat and mechanical power. Due to the volatility of photovoltaic and wind electricity, large scale energy storage systems are required to smooth the production curve and stabilize the net. A feasible implementation of renewable energies can be achieved by the transformation of energy into gases like hydrogen or methane (power-to-gas), into fluid fuels (power-to-liquid) or into other chemicals for the chemical industry (power-to-chemicals). In a research project the thermo-chemical storage of hydrogen will be investigated. The bachelor thesis described here will be developed in close relation to that project. In the bachelor thesis a numerical simulation of the fluid mechanics inside the storage system should be developed, which enables the determination of the pressure loss and temperature profiles in a vertical pipe filled with solid spherical pellets.

The following tasks are part of the work:

- Literature review of the state of the art in the modeling of fluid mechanics inside fixed beds (CFD, empiric) and the generation of geometries (particle resolved).
- Generation of a suitable geometry from DEM or empiric models and validation with a suitable reference from the literature.
- Development of a CFD model for determination of the pressure loss and validation with data from the literature or experimental data.
- Refinement of the CFD model to consider heat transfer. Temperature profiles should be modeled and validated from literature or experimental data.
- Consideration and evaluation of the effects of changes in the density or mass in the flow.
- Documentation of the results and preparation of a technical report.

Supervisor Professor:	Prof. Dr. Cornelia Breitkopf
Supervisor:	Dr.-Ing. Andreas Jäger / Dipl.-Ing. Oscar Baños
Beginning on: 01.10.2022	Deadline on: 28.02.2023

Dr. Andreas Jäger

Supervisor

ABSTRACT

Hydrogen is a promising energy vector which could be used as an alternative to conventional fossil fuels in energy transportation to reduce the greenhouse emissions as its energy can be 100% renewable and it only produces water when used. However, the production and storage processes of hydrogen make it not as economical, what makes the tendency in industry to palliate these emissions using capture methods, but these methods require space and are not suitable for all applications, for example mobility purposes. Alternative methods of storage are being researched to make hydrogen a reliable choice for these applications. Chemical reaction with water inside fixed bed reactors is one of them. For its study, CFD is a useful tool, which allows low-cost but accurate behavior predictions for a wide range of variations in the storage and release process. These behavior approximations are very useful to determine the optimal size and shape of the reactor and the pellets inside. However, the heavy computational effort of the most detailed models does not make it always the chosen option. The generation process of a fixed-bed reactor model filled with spherical pellets is presented and validated using theorical and experimental data from literature. This developed model is then compared against other simpler models and also with empirical models using the Ergun equation to study the accuracy difference and what the causes are.

KEY WORDS

Hydrogen storage, Fixed bed reactors, Computational Fluid Dynamics, Particle Resolved Model, computational cost.

INDEX

1 INTRODUCTION

According to Our World in Data [1], global energy consumption has increased in almost a 30.5% from 2000 to 2021, and the tendency says that human need of energy will continue increasing. Although it is true that renewable energies have gained importance during last decade, being the 28% of the global production in 2021 and the first half of 2022 according to the IEA (International Energy Agency) [2], main source of energy are fossil fuels [2]. The increase in demand translates, therefore, into an increase in the use of fossil fuels, that presents two major problems.

Fossil fuels are not only limited, they are also really unequally spread around the world. As reference, oil, one of the largest energy sources used nowadays, is found in important quantities in just a few countries, the 84.9% of its global reserves is distributed in 10 countries [3]. This makes fossil fuels very susceptible to global crisis, like the 2021 pandemic, after which the need of a rapid recovery derived in a sudden increase of energy demand, unbalancing the global energy market. Another example is the Russia's invasion of Ukraine in February of 2022. Russia is by far the world's largest exporter of fossil fuels, and after the invasion, many countries stopped their importations. At the same time Russia increasingly curtailed or even turned off its export pipelines. Events like these can easily change the internal and external situation of a country and produce enormous imbalances in the energy markets, as the ones seen in Europe's energy markets since 2021. According to the IEA, the price of natural gas reached record highs mostly as a consequence of the above mentioned events. This affected the prices of electricity and oil, whose price reached record highs, and, as a result, so did electricity in some markets, and also, oil prices hit their highest level since 2008 [2].

The other big drawback of fossil fuels is the greenhouse gases that they produce when used to generate energy. According to [4], the unusually fast increase in the temperature of the planet is caused by the huge amount of greenhouse gases released to the atmosphere by human activity. This global warming is the cause of the extinction of some animal species, natural disasters due to extreme weather, conflicts and human migrations [5]. Although the use of fossil fuels is not the only source of greenhouse gases, it is certainly a major one according to [5], reason why the restrictions imposed by governments to these flues emissions are increasingly harsh.

One of the most promising alternatives to fossil fuels are the renewable sources, however, high system prices and specially the elevated costs of installation and other system-related, hinders their progression and decrease their impact in energy prices.

One important inconvenient of renewable sources is its volatility. Photovoltaic and wind electricity are the two most important renewable sources behind hydroelectric [1], and they have a large dependence on external factors as the time of the day or the weather conditions, this make their production curve very unstable. A solution to this issue would be to store the energy not required in large-scale energy storage systems. That would smooth the production curve and stabilize the net, also increasing the rentability of renewable sources. This energy could be transformed into gases like hydrogen or methane (power-to-gas), into fluid fuels (power-to-liquid) or into other chemicals for the chemical industry (power-to-chemicals). This thesis will focus on the transformation of energy into gases (power-to-gas), specifically hydrogen.

Hydrogen and hydrogen-based fuels can play an important role in sectors where emissions are hard to abate, either because mitigation measures may not be available or because they would be difficult to implement, for example, mobility applications lack the required space and weight is a crucial factor concerning efficiency and safety.

	Hyundai Tucson (gasoline)	Hyundai Tucson FCEV (hydrogen from natural gas)	Hyundai Tucson FCEV (33% renewable California hydrogen)**	Hyundai Tucson FCEV (46% renewable California hydrogen)***
Gasoline vehicle emissions equivalent (MPG_{GHG})	25	38*	54	63
Global warming emissions per mile (g CO_2eq/mile)	436	286	202	173
Emissions reduction relative to gasoline		34%	54%	60%

*The EPA rating for the Hyundai Tucson FCEV is 49 miles/kilogram hydrogen.

**California law (California State Senate 2006) requires a minimum of 33 percent renewable hydrogen content.

***The Air Resources Board projects renewable hydrogen content in California for 2015 will be 46% (CARB 2014).

Figure 1-1. Comparison of CO_2 emissions of a Hyundai Tucson using gasoline or different sources hydrogen as fuel. Image taken from [6].

As can be seen in Figure 1-1, the same car model produces more than a 50% more CO_2 emissions using gasoline than using hydrogen produced using natural gas, another oil derivate. This happens due to the mitigation measures applied during the hydrogen production process that cannot be applied directly in the car.

However, one of the main reasons why hydrogen is not, at least by now, the main fuel used for mobility, is its difficulty to be stored (this is more extensively treated at section 3. 5.). A lot of research has been done to improve the methods well stablished in industry as well as to find new ones. The main storage method used nowadays is high-pressure cylinders (the principal characteristics of this method are reviewed at section 3.4.1). This method, nevertheless, has some drawbacks as the large space occupied by the tanks or the unsafe high pressures necessary to have a sufficient energy density, that makes it less competitive against traditional fuels. There are some promising methods being investigated trying to be feasible alternatives to gas tanks (these methods are treated in section 3.5). This thesis will be focused on the ones based in chemical reaction with water of iron pellets. This method is a promising alternative to gas cylinders, solving problems like high pressures or large volumes requirements (how this method works as well as its advantages and drawbacks compared to others can be seen at 0.).

The working principle is based on the chemical reduction of water to produce the hydrogen feeding the propulsion method. This reaction would take place inside a chamber (chemical reactor) filled with the iron oxide pellets with a fix position (the particles bed), the denomination for this type of reactor is “fixed bed reactor”.

Studies in the reactor characteristics, as its optimal diameter, the appropriate shape and size of the active parts, temperature distribution or effective velocity of the flow, are crucial to determine the most efficient reactor and to make it a competitive alternative to other methods. Due to the wide range of combinations, experimentation becomes costly and time consuming, in addition, information elucidated from the conventional measurement techniques is limited. So, the use of empirical or computational models is preferred for this purpose. The problem with empirical models is that a lot of the phenomena happening inside the reactor are ignored, as they are limited to what happened outside, loosing information about temperature, the reaction or local effects. In addition, the precision of these models decrease for reactors with small relation of diameters of reactor and particles (D/d), which is the tendency of fixed bed reactors in order to be more efficient [7]. For all these reasons, Computational Fluid Dynamics (CFD) models (section 3.3) are increasing its popularity in studies of fixed bed reactors, however, due to the complexity of its internal mathematics, CFD simulations require a great deal of computational effort, which leads to high simulation times and modelling costs, reason why traditional plug-flow models (section 3.2.) keep being chosen for plenty industrial applications due to its simplicity.

In this thesis, results of pressure drop obtained with analytic plug-flow model and CFD heterogeneous model of a small D/d ratio (<10) fixed bed reactor have been compared to determine the difference of accuracy between them. Also, a study of the CFD model has been made to determine the relevance of the distribution of temperature inside the reactor and the changes in density and viscosity indeed.

2 MOTIVATION

The development of alternative energy sources and carriers is not fast enough to replace fossil fuels and thus avoid the worst consequences of climate change. The global trend is that energy crises and natural disasters will continue to increase if nothing changes. This is why it is crucial to accelerate research and development of the renewable and sustainable part of the energy network. The tools used for investigation play a crucial role in the speed of progress, so research to make them more efficient and accurate is of great importance.

3 THEORY-STATE OF THE ART

3.1 FIXED BED REACTORS MODELS

A fixed bed reactor is a tube, usually cylindrical, filled with active elements such as particles, open foams, or structured inserts. The particles are often spheres, cylinders, or rings, but complex shapes with external flutes or grooves have been also used for specific applications. These particles or foams react with other phase, liquid, or gas, passing though the reactor. Fixed bed reactors are widely used in the chemist industry for heterogeneous catalysis, they are a key part of the processes like steam and dry reforming of methane, the oxidative coupling of methane to ethylene, or the Sabatier process [8].

Studies to accurately predict the behavior of fixed and packed bed reactors began in 1990 and many models were developed, as the pseudo-homogeneous or the homogeneous model, which obtain really accurate approximations of reactors with a big D/d ratio.

Because most of reactions taking place inside them are either exothermic or endothermic, is desirable to have good control over temperature, and, at the same time, maintain an optimal surface contact surface between the phases and low pressure drop. This leads to small D/d ratio reactors, typically 3–10 [7]. However, traditional plug-flow pseudo-empirical models do not consider wall local flow effects or the uneven temperature distribution, events that have a dramatic influence on fluid dynamics in reactors with this characteristics [9]. As consequence, these models do not offer a good approximation of critical design variables of the reactor behavior.

To make models that would consider those uncertain effects, was later possible thanks to the implementation of a new tool that allowed calculating the two- or three-dimensional interstitial by solving the Navier-Stokes equations for a detailed representation of the bed structure. This new tool was Computational Fluid Dynamics (CFD) and it allowed to create 2D and 3D representations of the velocity and temperature fields inside the reactor, information that remains hidden for traditional models, and at the same time offering more accurate approximations of variables as the pressure drop across the packed bed. The limiting factor however was, for many years, the large computational effort that spoused huge number of operations required by the simulations. First models were in two dimensions (and still widely used in industry due to its simplicity) [7], but thanks to the improvements in software and hardware during its twenty five years of development, it has become much faster and affordable [9] allowing to create 3D representations even in regular computers.

Principal characteristics

In the model of a fixed bed reactor three principal scales have to be considered, the molecular scale to determine the parameters of the chemical reaction, the particle scale to study the diffusion experimented by the fluid inside the porous media, and the reactor scale where flow, mass and heat transport are evaluated [8].

According to the detail in the bed geometry representation, a model can be classified as homogeneous, pseudo-homogeneous or heterogeneous. Homogeneous reactor models are those in which the radial distribution of porosity is not considered, and all the catalyst phase is taken as a continuous medium with the same porosity. Pseudo-homogeneous models are those that consider the radial porosity variation by increasing the value of porosity near to the walls. Heterogeneous model considers explicitly the presence of the catalyst phase [8].

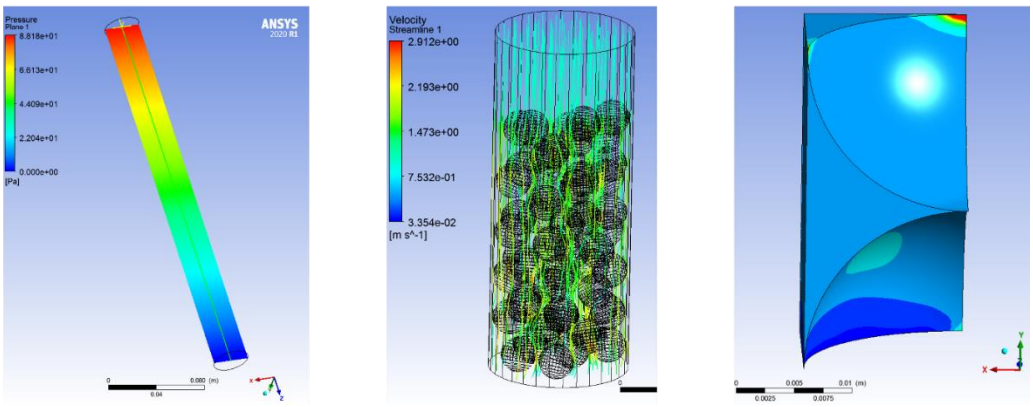

Figure 3-1. Image of two models from reactor scale models one homogeneous (left), one heterogeneous (center), and one heterogeneous from particle scale (right).

3.2 PLUG-FLOW MODELS:

Plug-flow models are the simplest ones and therefor very used in industry when it is possible [8]. In these models, a radially uniform and constant velocity field is assumed. As these models do not consider radial variations in porosity and velocity or longitudinal variations in temperature, they do not offer good approximations for reactors with small D/d ratio, as those are phenomena with great influence in these cases [8]. Many semi-empirical correlations have been experimentally determined to be used in these models to improve its accuracy, however these correlations are

determined for specific particles shapes, temperatures or velocity flows, so they are not applicable for all cases [8].

The equations to calculate the pressure drop across the packed bed of two plug-flow models are shown below.

3.2.1 Pressure Drop Equations Based on the Model of the Hydraulic Diameter:

The Ergun equation is a correlation typically used to predict the pressure drop in fixed bed reactors. It is based on a model that considers the fixed bed as set of parallel pipes through which the fluid flows and the pressure loss is analogously calculated to that for single-phase pipe flow, being the hydraulic diameter of the bed the characteristic pipe dimension [10]. The particle bed is characterized using the Sauter-diameter d_p, it is the characteristic particle diameter and can be calculated for non-spherical pellets using the Equation 3-1 [10].

$$\overline{d_p} = \left[\sum_{i=n}^{n} \frac{V_i}{V} * \frac{1}{d_{pi}}\right]^{-1}$$

Equation 3-1. Equivalent diameter

Being d_{pi} the average diameter of the particle i. For a better approximation, the equivalent Sauter diameter can be multiplied by a correction factor, the pressure drop shape factor ϕ_d, which is experimentally obtained for specific shapes and materials. Equivalent Sauter diameter $\overline{d_p} * \phi_d$.

$$\frac{\Delta P}{\Delta L} = 150 * \frac{(1-\varepsilon)^2}{\varepsilon^3} * \frac{\eta * v}{\overline{d_p^2}} + 1.75 * \frac{1-\varepsilon}{\varepsilon^3} * \frac{\rho_f * v^2}{\overline{d_p}}$$

Equation 3-2. Ergun equation

The two constants in the Ergun Equation depend on the shape and the porosity of the particles and can be varied to fit an experimental result. Equation 3-2 is the general form of the Ergun Equation.

In Equation 3-2, the first part of the equation on the right side determines the pressure drop in viscosity-controlled flow, the second part determines the pressure drop due to the inertia-controlled flow. However, the pressure drop produced by the boundary layer, the zone of interaction between the fluid and solid phases, is not considered in Ergun equation [11].

The main drawback of the Ergun equation is that the model of the hydraulic diameter can only be used in the turbulent region, the inertia-controlled flow. It is not correct to use this model for the laminar flow region, where flow is controlled by viscosity. Therefore, it is not appropriate to apply it to fixed beds consisting of fine-grained solids, with small Reynolds along the bed.

The Carman–Kozeny equation is a special case of the Ergun equation which can only be applied in regions where the fluid viscosity controls the pressure drops, laminar regions. A generalized form of the Carman–Kozeny equation is the Darcy equation.

$$\frac{\Delta P}{\Delta L} = \frac{1}{B} * \eta * v$$

Equation 3-3. Darcy equation

The permeability B must be determined experimentally for each fixed bed.

3.2.2 Pressure Drop Equation Based on the Model of the Flow Around Single Particles:

This models is based in the resistance W_1 experimented by the fluid when it flows around a particle [11]. The flow resistance W_1 of each particle in the fixed bed passed through with the average interstitial velocity $\frac{v}{\varepsilon}$, is characterized by the dimensionless Euler number [11]:

$$Eu \equiv \frac{4}{3} * \frac{\Delta P}{\rho_f} * \frac{\overline{d_p}}{\Delta L} * \frac{\varepsilon^2}{1-\varepsilon} = \frac{W_1}{\frac{\rho_f}{2} * \frac{\overline{d_p^2} * \pi}{4} * \left(\frac{v}{\varepsilon}\right)^2}$$

Equation 3-4. Euler Number

By combining the Navier-Stokes equations with the this analisys of the flow and pressure drop measurements, Molerus obtained the Equation 3-5 to determine the Euler number for spherical particles [11]:

$$Eu \equiv \frac{24}{Re} * \left\{1 + 0.692 * \left[\frac{r_0}{\delta} + 0.5 * \left(\frac{r_0}{\delta}\right)^2\right]\right\} + \frac{4}{\sqrt{Re}} * \left[1 + 0.12 * \left(\frac{r_0}{\delta}\right)^{1.5}\right] + \left[0.4 + 0.891 * \frac{r_0}{\delta} * Re^{-0.1}\right]$$

Equation 3-5. Euler Number for spherical particles

Being

$$\frac{r_0}{\delta} = \left[\frac{0.95}{\sqrt[3]{1-\varepsilon}} - 1\right]^{-1}$$

Equation 3-6. $\frac{r_0}{\delta}$

The packing structure of the fixed bed is defined by Equation 3-6. $\frac{r_0}{\delta}$ and is valid for uniform random packing.

And the Reynolds number (Re) for particle diameter is determined by the expression:

$$Re \equiv \frac{\rho_f * v * \overline{d_p}}{\varepsilon * \eta}$$

Equation 3-7. Particle Reynolds Number

The Stoke-flow around the particles is characterized by the first part of Equation 3-5. The flow resistance produced by the boundary layer of the fluid flow at the surface of the particles is characterized by the middle part of this equation. The last part represents the separation characteristics of the fluid flow around the particles. Unlike the previous model, this one considers the boundary layer around the particles of the fixed bed whereas it still not considering the changes in temperature of the fluid so neither the changes in its density and viscosity [11].

3.3 CFD:

Computational Fluid Dynamics is a method where derivatives of Navier-Stokes equations are simulated by algebraic relations between a finite number of grid points in the flow field, which are then solved on a computer. [10] This method manages to overcome the uncertainty in the effective parameters as they are solved in the equation for each point in the reactor [8].

3.3.1 Porous Medium Approach:

The porous medium model (PMM) considers the fixed bed as a continuum medium, as it does not consider the explicit presence of the particles, the momentum loss due to them must be included through source terms. These source terms, including the viscous loss resistance and inertia loss resistance, are added to the incompressible Newtonian fluid Navier-Stokes equations. However, source terms cannot reproduce the axial flow variations due to the oscillating porosity profile,

which for certain types of reactors can have an important impact. If axial porosity changes are wanted to be implemented to the model, usually the void factor distribution ε(r,z) is chosen, however to accurately determine this factor, a measure of the bed must be made. Often the axial variation is neglected, and the oscillating void factor is replaced by an exponential function which only represents the increase in voyage close to the reactor's wall.

The main advantage of this method is that it presents a higher accuracy than plug-flow models at the same time the computational effort is relatively low compared with the particle-resolved CFD. In the comparison made in [12] between Particle-Resolve CFD (PRCFD) to the porous medium approach. They noted a lack of accuracy of the PMM as it cannot reproduce secondary flows and neither flow anisotropies as vortex formations. In the other hand PMM proved to be able of capturing average pressure drop and temperature increase, all with a computational cost 3000 times lower than the particle resolved CFD.

The relatively accurate prediction in the pressure drop happens because of the average radial symmetry of the bed, causing that many variations in axial velocity cancel out with another in the opposite radial-coordinate (r). This makes not notable effect on pressure drop when radial velocity is neglected [7].

3.3.2 Particle-Resolved Computational Fluid Dynamics Model:

The usual workflow for these methods consists in creating a calculation domain based on the particle position data from a random packing, usually generated using the discrete element method (DEM). The calculation domains, including the particles and the voids between them are volume meshed. Then, the model is solved by continuum Navier Stokes approaches, as finite volume (FV) or finite element (FE), and particle-based approaches, as the Lattice Boltzmann method (LBM).

The continuum methods used in most CFD software, as the one used in this thesis ANSYS®-Fluent, solve the conservation equations of macroscopic quantities in the form of the Navier-Stokes equations, applying the FV approach. These equations are defined on a discretized region of space on a mesh (along with time for unsteady flows) [7].

The advantages of PRCFD above classical approaches are that no correlations for effective parameters are needed and, as it allows algorithm-based design, development and optimization of new catalyst pellet shapes would be possible without experimentation [7]. However, due to the high computational cost of these models, there are commonly used to provide data and parameters to be used in simpler models, improving their accuracy [7].

3.3.2.1 Packing generation

Reconstructive methods:

The digitalization of the mesh is made by magnetic resonance imaging (MRI) or X-ray microtomography (XMT). It is usually expensive and time consuming [9].

Idealized particle arrangements:

It is the simplest kind of bed generation, which consists in an explicit mathematical description of the position of each individual particle can be derived. It is a good way of representing geometries with low computational effort but porosities of beds arranged this way differ with randomly arranged ones.[9]

Random particle arrangements:

- **Monte Carlo method:**
  This method consists in the random initialization of particles inside a domain and then statistically move them to a position where overlapping is avoided and the void fraction minimized. Collisions of the particles are not considered in this method, what leads to unrealistic nonphysical pellet arrangements, especially for non-spherical particles or if other bodies exist inside the reactor, being this the principal drawback of this method [9].

- **The deterministic discrete element method (DEM):**
  Results obtained with this method have shown to be more realistic than with the previous, it consists in simulate the move of discrete particles interacting between them and with the surrounding environment [9]. This method can be found in numerous commercial software packages (like STAR-CCM+, ROCKY DEM, EDEM, or PFC) and open-source codes like LIGGGHTS or YADE-DEM [9]. One of the main advantages of this method is that can be used to obtain physically realistic arrangements even with non-spherical pellet (e.g.

cylindrical, trilobe) [9]. The soft-sphere model is the more generally used and in it the particles can overlap with other surfaces, but the contact forces are proportional to the overlap and other particle properties as the geometry or the material, this leads to realistic stationary state with the minimum overlapping [9].

3.3.2.2 Micro kinetics:

Reaction is not considered in this thesis, but its effects can be considered with the micro-kinetics model. The micro-kinetics model provides a detailed reaction mechanism that is utilized to calculate the surface flux of each species based on the temperature and partial pressures of the species at the solid-fluid interface. These surface flux values are then employed as boundary conditions for the flow field on the interface between the fluid and solid [7].

3.3.2.3 Contact points:

Contact points between particles or either particles with the wall are a problem in the PRCFD models. It is relatively simple to solve with spheres where only point contacts exists, but it gets a lot more complex with cylinders and other particles shapes where also line or area contacts exist. In the mesh around these zones, the fluid cells can be distorted or very small due to the little distance between walls, what traduces in large cells numbers and more complex calculations, increasing the computational time and effort.
Contact points can be eliminated by different methods, like modifying the particles shape and size, or by constructing bridges between them, occupying the volume where the fluid cells would be too small [7].

3.3.3 Meshing:

In order to be solved by a CFD algorithm, the geometrical domain needs to be discritized into smaller regions through meshing [7]. The mesh is used for the main calculation domain including both fluid and solid regions, it determines the accuracy and reliability of a CFD simulation. The choice of the type and size of a mesh will depend on a trade-off between accuracy and computational efforts, so a mesh study is required in a CFD simulation to determine the maximum size of the mesh without variations in the result for larger sizes [8].

In this thesis, a dense polyhedral volume mesh is used for the main calculation domain, including both fluid and solid regions. This type of mesh is preferred over tetrahedral mesh for solving conjugate heat transfer problems because its flexibility to have a larger number of neighboring cells and more accurate gradient approximation [8].

3.3.4 Fundamental equations:

The set of governing equations for solving the laminar flow through the heterogeneous catalytic reactor, neglecting reaction and assuming steady flow, include the Navier-Stokes equations (conservation of mass and momentum) and conservation of energy [13].
All the simulations presented in this thesis were carried out neglecting gravity and in stationary state, so gravity and time depending terms of the equations are omitted.

$$\frac{\partial}{\partial t} \equiv 0$$

Equation 3-8. Stationary State Assumption

3.3.5 The Mass Conservation Equation:

From the Eulerian frame of reference, the velocity vector depending on position is [10]:

$$\vec{v}(r) = iu(x,y,z) + jv(x,y,z) + kw(x,y,z)$$

Equation 3-9. Velocity vector

The equation for conservation of mass, or continuity equation, can be expressed as follows:

$$\frac{\partial}{\partial x}(\rho u) + \frac{\partial}{\partial y}(\rho v) + \frac{\partial}{\partial z}(\rho w) = 0$$

Equation 3-10. Equation for mass conservation

Being:

$$\nabla = i\frac{\partial}{\partial x} + j\frac{\partial}{\partial y} + k\frac{\partial}{\partial z}$$

Equation 3-11. Vector gradient

It can also be written as:

$$\nabla * (\rho \vec{v}) = 0$$

Equation 3-12. Equation for mass conservation

Being ρ the fluids density also depending in position [10].

3.3.6 Momentum Conservation Equations

Conservation of momentum in an inertial (non-accelerating) reference frame is described by [13]:

$$\nabla(\rho * \vec{v}\vec{v}) = -\nabla \mathrm{P} + \nabla(\bar{\bar{\tau}}) + \vec{F}$$

Equation 3-13. Equation for momentum conservation

Being P the static pressure, $\bar{\bar{\tau}}$ the stress tensor (Equation 3-14) and $\vec{F}$ the external body forces which also contains other model-dependent source terms.

The stress tensor is defined by:

$$\bar{\bar{\tau}} = \eta[(\nabla \vec{v} + \nabla \vec{v}^{T}) - \frac{2}{3}\nabla \vec{v} I]$$

Equation 3-14. Stress tensor

Where η is the dynamic viscosity, I is the unit tensor, and the second term on the right-hand side is the effect of volume dilation.

3.3.7 The Energy Equation

Ansys Fluent solves the energy equation in the following form [13]:

$$\nabla * \left(\rho * v \left(h + \frac{v^2}{2} \right) \right) = \nabla * \left(k_{eff} * \nabla T - \sum_j h_j \vec{J_j} + \bar{\bar{\tau}}_{eff} * \vec{v} \right) + S_h$$

Equation 3-15. Energy equation

Where k_{eff} is the effective conductivity, $k + k_t$, where k_t is the turbulent thermal conductivity, defined according to the turbulence model being used, as in this thesis turbulent flow is neglected

$k_{eff} = k$. J_j is the diffusion flux of species j, in the cases seen in this thesis there is not diffusion. The first three terms on the right-hand side of the equation represent energy transfer due to conduction, species diffusion, and viscous dissipation, respectively. S_h represents volumetric heat sources that you have defined and the heat generation rate from chemical reactions, but neither of these effects are considered in the simulations made in this thesis.

The enthalpy is defined for incompressible materials as:

$$h = \sum_j Y_j h_j + \frac{P}{\rho}$$

Equation 3-16. Enthalpy for incompressible materials

For ideal gases is defined as:

$$h = \sum_j Y_j h_j$$

Equation 3-17. Enthalpy for ideal gases

Where Yj is the mass fraction of species, in the simulations made in this thesis there is only one specie, $\mathrm{Y} = 1$. Sensible heat of species h_j is the part of enthalpy that includes only changes due to specific heat.

$$h_j = \int_{T_{ref}}^{T} c_{p,j} dT$$

Equation 3-18. Sensible heat of species

For density-based solver T_{ref} is 0 K when reaction is not modeled.

3.3.8 Fluid-Particle Coupling

For heterogeneous catalytic reactor simulations is important to include chemical species inside the particle in order to get an accurate model of the reaction.

A first approach can be done treating the particles as porous regions, the drawback of this approximation is that allow too much convective heat and mass transfer into the particles [7].

A better approach would be model the particles as solid regions and employ user-defined scalars to determine the mass fractions of species inside the particles[7]. Maestri & Cuoci [14] came up

with a different approach to solve large sets of species balances combining micro-kinetics reactions with CFD simulations. They separated the fluid transport and particle reaction timescales using an operator-splitting technique [7].
As in this thesis reaction is not simulated, fluid-particle coupling effects have been neglected in the simulations.

3.4 HYDROGEN STORAGE

Hydrogen is a suitable element to be used as an energy vector, which means that it can be used to store and transport energy. Now a days it is one promising alternative to fossil fuels, as it only produces water vapor when it is used to generate electricity or power vehicles. One of the great advantages of using hydrogen to store energy is that this energy can be 100% renewable.
Even though hydrogen is relatively abundant on earth, it is rarely found in pure state, whereas it is found in the form of hydrocarbons and water, so it must be produced, this can be done using a variety of renewable energy sources such as solar, wind, and hydro power or using fossil fuels through processes like steam reforming with natural gas or gasification using coal or oil. This is the first drawback because the costs of getting pure hydrogen and store it are higher than the ones of extracting fossil fuels which only requires a relatively cheap transformation to be ready to use. All this, in most cases, make hydrogen a less economical option [15].
Furthermore, most of the hydrogen consumed nowadays is produced by the fossil fuels consuming methods, it is called “gray hydrogen” and is largely cheaper than the one produced by renewable sources energy called “green hydrogen”. The issue with this type of hydrogen is, that even though when this hydrogen is used, no greenhouse gases are produced, the processes to obtain have already produced almost the same amount of CO2 as if the fossil fuels used were directly burned to produce electricity. This can be appreciated in Figure 3-2.

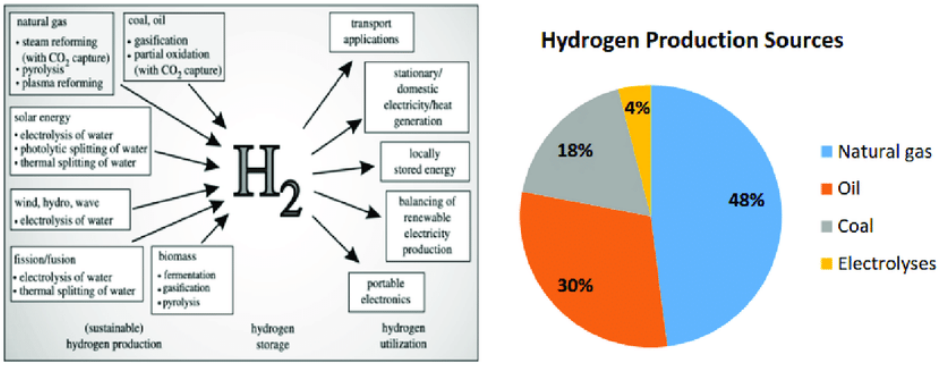

Figure 3-2. Hydrogen production methods [16].

An interesting idea, which deals with the issue of elevated prices of hydrogen due to its production, consist in using energy, that otherwise would be wasted, to produce hydrogen. For example, hydrogen can be used too to decrease the discoordination between electricity production and demand in actual networks, especially with renewable energies, as some of them like solar or wind depends largely on external incontrollable factors that makes them very irregular. Storing the energy by producing hydrogen by electrolysis when demand is lower than production and using it for other applications, or to produce electricity when demand is higher, would increase the efficiency of the electrical networks and the profitability of renewable sources as well as it would decrease the price of hydrogen [17].

The reason of choosing hydrogen over other elements to this purpose is because it has the highest electrochemical potential of all elements, the fact that it only has one electron in the lowest energy level, one proton and one neutron, makes relatively easy for the electron to be pulled away from the atom. This and the fact that hydrogen is the lightest element makes it the one that the greatest amount of energy per unit of mass consumed produces in a red-ox reaction, what makes it very efficient for a galvanic cell or to be burned in a combustion chamber [15].

For energy storage in hydrogen to be 100% renewable the energy used to produce it must come from renewable sources (solar, wind, hydro, wave…). This energy can come in terms of electricity, for electrolysis of water, or heat for thermal water dissociation H2O → H2 + 1/2 O2 at 2.500 K. But this hydrogen called green hydrogen is almost 3 times more expensive. According to the International Energy Agency (IEA)[2], "Depending on regional gas prices, the average cost of hydrogen production from natural gas ranges from USD 0.5 to USD 1.7 per kilogram (kg). Using CCUS technologies to reduce the CO2 emissions from hydrogen production increases the average cost of production to around USD 1 to USD 2 per kg. Using renewable electricity to produce hydrogen costs USD 3 to USD 8 per kg".

The storage and transport of hydrogen is other big problem of using it as energy carrier. Hydrogen has a great gravimetric density (ratio of the mass of hydrogen stored within the metal or compound to the mass of the host material including the hydrogen (wt%)[15]), but an inconvenient volumetric density (mass per unit volume), at a temperature of *0°C* and a pressure of 1 bar, hydrogen is found in gas state with a density of *0.089886 kg/m3*. This very low density means that, for storage and transport of hydrogen gas to be feasible, an enormous reduction on its volume has to be done. In other to increase hydrogen density, it must be compressed, or its temperature must be decreased below the critical point (T_c = *33 K* Figure 3-3).

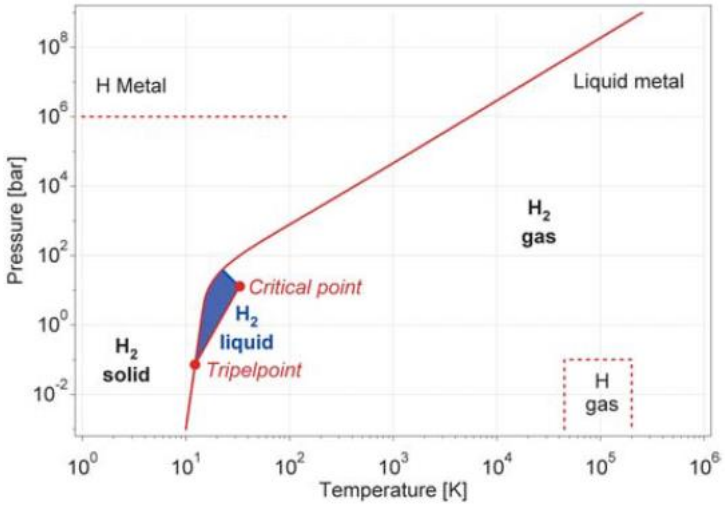

Figure 3-3. Phase diagram for Hydrogen [15].

Other way of getting lower densities is to reduce the repulsion between its molecules, which is the cause of its very low critical point, this can be achieved by the interaction of hydrogen with another material.

Besides, maintaining hydrogen in the desired state, brings other drawbacks as for example complex thermal management systems, boil-off, poor efficiency, expensive catalysts, stability issues, slow response rates, high operating pressures, and risks of violent and uncontrolled spontaneous reactions [5]. The work necessary to deal with these obstacles increase the cost of energy in hydrogen, that is why suitable methods to storage hydrogen are being widely researched.

Hydrogen storage technologies:

As the reactor studied in this thesis is thought to be used as a part of the storage system of a hydrogen-powered vehicle, from this point on, the storage methods description will be focused on mobility applications.

For mobility purposes, the are some crucial characteristics that define the ideal storage system, like high gravimetric and volumetric energy densities, fast refueling what leads to fast reaction kinetics, safety is of prime importance, and weight and size as low as possible [5].

The most used methods for hydrogen storage are:

3.4.1 High-pressure gas cylinders:

Is the most common storage system in energy and automotive industry, maximum value for the pressure comes mostly determined by tree factors, the most important is the user's safety, so the tanks must accomplish the regulations stipulated. Other factor is the gravimetric density of the tank, at higher pressures the walls of the container became thicker, and the gravimetric density decrease so an equilibrium must be found. According to [15], the gravimetric density of high-pressure gas cylinders is *13 wt%* at pressure of *800 bar*. However, the gravimetric density that can be found actually at the market is around *5.7 wt%*. This happens because of the *4.1 wt%* energy taken to compress hydrogen and to the required pressure and to the *1.8–3.6 wt %* used to avoid tank overheating while refilling [5]. Due to the extremely high pressure, the shape of the tank must be a cylinder, what complicates its installation in the vehicle. The most used materials for the tank construction are nnylon-6 and carbon fiber, these materials are not toxic or environmentally harmful, however the high pressure of the hydrogen inside can be dangerous[5].

3.4.2 Liquid hydrogen:

Liquid hydrogen, stored in tanks at *21.2 K* at ambient pressure, must be continuously cooled and very well isolated because there is not liquid phase above its critical point (*33 K*). As a reference, the maximum volumetric and gravimetric energy densities inside a hypothetical tank with spherical shape and *25 mm* of insulation material, would be of *6.4 MJ/L* and *7.5 wt%*, respectively [5]. The large amounts of energy and resources, required to maintain hydrogen in liquid form, and the boil-off losses make this technology more expensive than the other alternatives, limiting its use to applications where cost is assumed in favour of performance, such as the aerospace industry [15].

3.4.3 Physisorption of hydrogen:

The dispersive interactions or Van der Waals interactions creates a field force at the surface of a solid, called the adsorbent, which attracts the molecules of a gas or vapor, called adsorbate, this phenomenon is known as adsorption [15]. As only physical forces are involved, it is called physisisorption. In the case of hydrogen, due to the weak interaction, a significant physisorption is only observed at low temperatures (*<273 K*) [15]. The potential storage capacity of simple wall carbon nanotubes has been calculated with Monte Carlo simulations. The storage capacity predicted at *298 K* and *100 bar* was slightly lower than *10 wt% [5]*.

Experimental data reported by Ariharan et al. [18], using synthesized carbon nanotubes doped with nitrogen, was of a reversible storage capacity of *2.0 wt%* at *298 K* and *100 bar*, the storage capacity is too modest for it to be a significant change. Data reported by Masika and Mokaya [19] of *7.3 wt%* at *20 bar* and *77 K* using zeolite templated carbon, shown interesting gravimetric densities, however temperatures are too low to be used for mobility purposes.

"The Chahine rule is a widely accepted concept which states that, in general, there is *1 wt%* hydrogen adsorption for every *500 m^2/g* of surface area" according to [5].

3.4.4 Metal hydrides:

Hydrogen generally reacts with metals, intermetallic compounds, and alloys, forming compounds (metal-hydrogen) [15]. This method is based in the reaction happening of hydrogen gas with a metal, called the absorption [15]. According to [5] "The maximum volumetric density of hydrogen in a metal hydride, assuming a closed packing of the hydrogen, is therefore *253 kg/m^3*, which is 3.6 times the density of liquid hydrogen". The process used to remove the hydrogen from the metal is called desorption and is carried out applying heat, pressure or both depending on the process. Magnesium hydride is an abundant and affordable material with a density of *1.45 g/cm^3* and energy densities *7.6 wt %* and *13.22 MJ/L* respectively, all this make it attractive to be used for hydrogen storage [5].

Yahya and Ismail [20] report a storage capacity of *6.1 wt%* in *1.3 min* at *320 ◦C* and *27 bar* using an Ni composite. According to [21] sodium aluminum hydride (NaAlH4) show a lower capacity of *4.9 wt%.*

Even though metal hydrides are very effective for the storage of large amounts of hydrogen, the high temperatures and slow kinetics involved in the fueling and release processes are important drawbacks for reversible storage [5].

The efficiency of this method is significantly reduced by the losses during fueling and release, plus, bulk isolation is needed what increase the weight of the system. Another issue of this method is the high reactivity of some of hydrides like magnesium with air or water [5], making them not safe to use for mobility applications.

3.4.5 Complex hydrides:

The light elements in group one, two and three, such as Li, Mg, B, and Al, form numerous metal-hydrogen complexes. Due to their lightweight and the high ratio of hydrogen atoms to metal atoms, they are considered a promising option for mobility-related purposes .

This method presents relatively high storage capacities with gravimetric densities from *14.9 wt %* to *18.5 wt %* and volumetric energy densities between *9.8 MJ/L* and *17.6 MJ/L* [5].

One of the most investigated borohydrides is the lithium borohydride ($LiBH_4$) which shows large storage capacities, however, temperatures involved for hydrogenation and dehydrogenation are high and its kinetics slow [5]. Besides, intermediate compounds are formed during reaction steps making its reuse an issue.

The nonporous hydride γ-$Mg(BH_4)_2$ does not present this problem with reversibility, Ley et al. [23] reported a gravimetric density of *17.4 wt%* at *105 bar* and *-143 °C*. However, the extremely low temperature involved would suppose thermal management.

Since most of the complex hydrides do not exist as intermetallic compounds when the hydrogen is removed, very little is known about the stability, the sorption kinetics, and the reversibility [15].

3.4.6 Kubas-Type Hydrogen:

The Kubas-type interaction is a chemisorption that happens at the surface of the transition metals. Was reported in an experiment with a manganese hydride molecular sieve made in [24], promising values of *10.5 wt %* and *23.64 MJ/L* at *120 bar* and ambient temperature. The reaction is independent of the temperature and the pressure variation is relatively low. Although the results are promising, they have to be corroborated [5].

3.4.7 Liquid Organic Hydrogen Carriers:

This method consists in hydrogenate an organic compound in orther to store hydrogen and then dehydrogenate it when the hydrogen is needed [5]. It is much easier than managing compressed gas. One of the most studied compounds is dodecahydro-N-ethylcarbazole. When dehydrogenated it becomes N-ethylcarbazole. It has a theoretical maximum storage capacity of *8.5 wt*% hydrogen and *7 MJ/L* [5], quite similar to liquid hydrogen (3.4.2). Other important compound is methylcyclohexane (MCH), which contains 6 more hydrogen atoms than toluene, with the potential to release *6 wt%* hydrogen or *5.5 MJ/L* when converted to toluene. However, the toxicity of MCH become a significant issue in its use for mobility purposes. Another LOHC which is being studied and evaluated is the dibenzyltoluene, which can store up to *6.2 wt%* at *7.7 MJ/L* of hydrogen [5].

The main drawback of using LOHCs for mobility purposes is the highly endothermic and exothermic nature of the hydrogenation and dehydrogenation reactions respectively. This fact makes them much more suitable to be used for applications in which this large amount of heat can be utilized or supplied [5]. Additionally, this processes requires expensive precious metal catalysts which, besides, degrades relatively soon, its activity decrease from 94% to 81% over a period of 82 h [5].

3.4.8 Chemical reaction with water:

Hydrogen can be obtained from the reaction of metals and other chemical compounds with water [15]. Methane and ammonia are suitable to produce hydrogen through water electrolysis, but the processes are too complex to be implemented in a vehicle [5]. Therefore, a better way of using them as fuel is through solid oxide fuel cells directly, the problem is that catalyzers in these cells are precious metals which are decomposed in a few cycles, making this alternative very expensive for mobility process [5].

Another interesting way to produce hydrogen through chemical reaction with water, is by using iron oxides, this method is extensively explained below since it is a suitable application for the reactor modeled in this thesis.

Reduction of Iron Oxides:

In this storage method, when the system requires hydrogen, water would pass through a reactor filled with small Iron pellets oxidizing Iron and obtaining pure gaseous hydrogen. Both reduction and oxidation reactions can be seen at Figure 3-4.

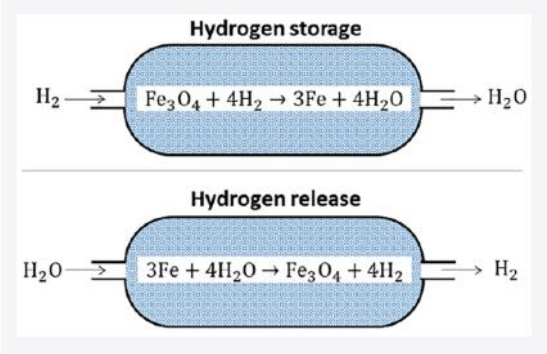

Figure 3-4. Reduction and oxidation reactions inside the fixed-bed reactor for hydrogen storage and release, respectively [26]**.**

The usage of this technology for mobility applications can be seen in the FEREDOX technology developed by NACOMPEX® [25]. A diagram about how this technology works can be seen in Figure 3-5. The main parts of the power system of the vehicle would be a galvanic cell for water electrolysis and a fixed bed reactor with an Iron pellets bed, so with system charged, water steam proceeding from an evaporator would go through the reactor oxidizing the iron pellets. As products of the reaction a stream of hydrogen and water steam would be obtained, this mixture would power an internal combustion engine which would power an electric generator to power the wheels. As product of the combustion a stream of water steam would be gotten and conducted to the fixed bed reactor for repeating the cycle.

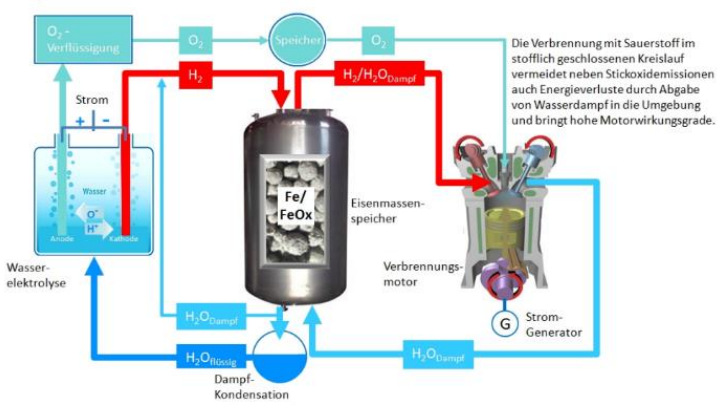

Figure 3-5. FEREDOX project by NACOMPEX® [25].

Once iron in the reactor is oxidized, the recharging process would consist of passing a current of hydrogen through the reactor to reduce the FeOx to Fe. This hydrogen would come from the electrolysis that occurs in the galvanic cell, as it is connected to an external electricity source. As another product of electrolysis, gaseous oxygen would be stored in a deposit to be later used to improve the combustion in the engine.

According to an experiment made by [26] a packed bed formation of iron pellets with a density of *2 kg/L* would have a gravimetric density around *5 wt%,* its volumetric density is relatively high when compared with the other methods, meaning it can storage more hydrogen in a reduced space, whereas its gravimetric density is relatively low, the percentage in weight of the system occupied by hydrogen is lower than in other methods. This is graphically represented at Figure 3-6 from the study made in [26].

The main advantage of this method above the other storage options is the relative low pressure required, the thermodynamics of iron redox cycling are independent of pressure, and the kinetics activity is reasonable over a wide pressure range [26]. The temperature is a more critical process condition, oxidation should be performed in the temperature range $T = 100{-}500\ °C$ and reduction, temperatures above $400\ °C$ were more favorable for a low energy demand. These relatively high temperatures could be a considerable drawback.

About kinetics, the estimated time required to reach 50% conversion of the solid phase, at around $400\ °C$, is between 5 and 100 minutes. Iron with additional support materials, such as MoO_2 and Al_2O_3, generally shows faster kinetics and maintains higher rates at lower temperatures than pure iron. It is likely that kinetic rates would have been higher at higher vapor pressures [26].

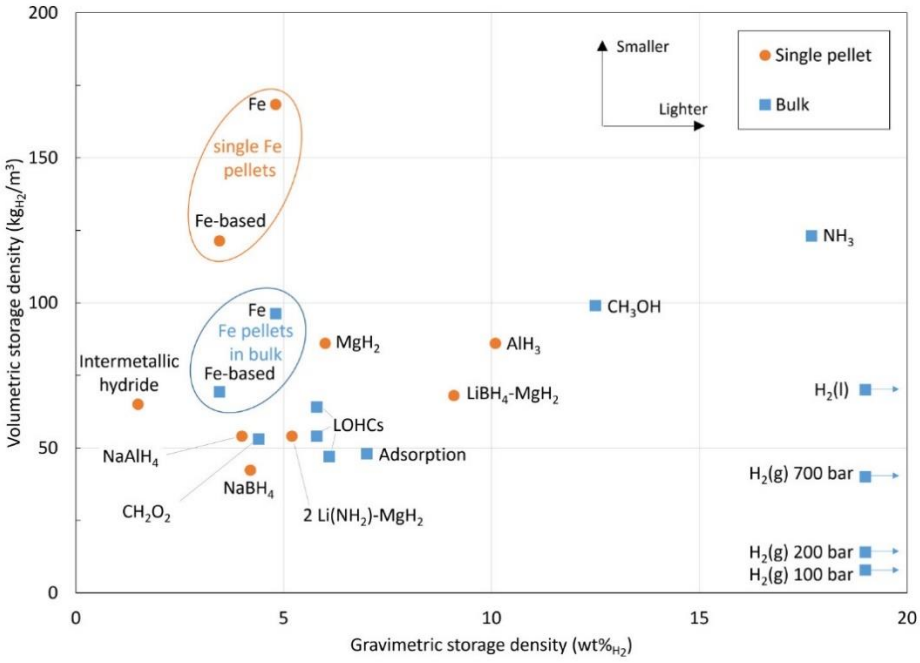

Figure 3-6. Different storage methods represented according to their volumetric (Kg_{H2}/m^3) and gravimetric densities ($wt\%_{H2}$) [26].

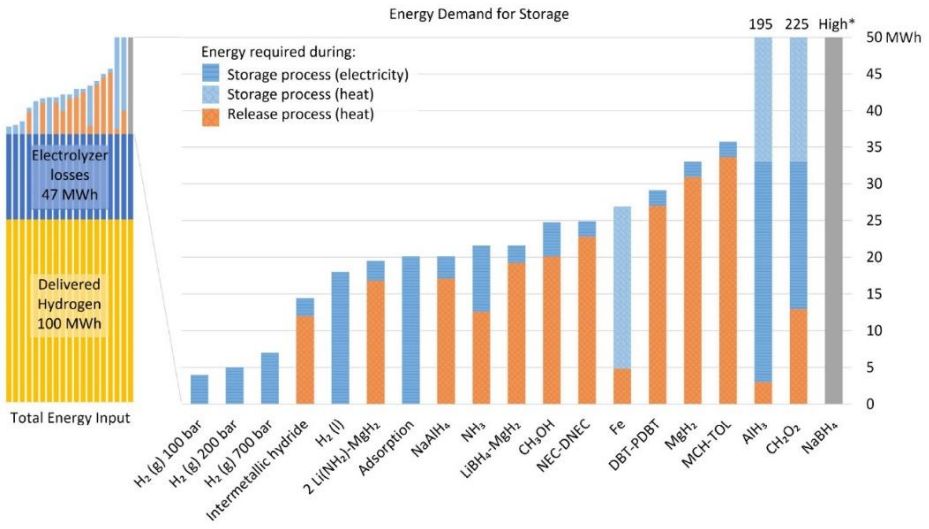

Figure 3-7. This graphic shows the energy demands for producing and storing *100 MWh* of green hydrogen for selected hydrogen storage technologies. It is assumed that the hydrogen is produced with an electrolysis efficiency of 68% [26].

In Figure 3-7 [26] can be seen how due to the heat involved in the release and specially in the storage process, the chemical reaction with iron oxides method has relatively low efficiency in

energy terms when compared with other storage methods, being storage inside high pressure tanks the one with less energy waste.

Conclusion

The iron oxides method is suitable to be used for mobility applications because of the relative low pressures and temperatures required in the processes, the high volumetric density, cheap use and maintenance and relative fast kinetics. However, research is needed to find fixed bed reactors able of higher gravimetric densities for it to be a feasible alternative.

4 FIXED BED REACTOR MODEL GENERATION AND VALIDATION

The model developed in this thesis is a fixed bed reactor model with a small diameter correlation (D/d<10), the bed is composed by spherical pellets randomly packed using the DEM. As there was not possibility of self-obtaining experimental data for a reactor with these characteristics, the model had to be validated thought comparison with theorical and experimental data from the literature [8]. In other to compare the results, geometry and flow conditions from the experiment made in [8] were taken as reference for the model. These conditions can be seen in Figure 4-1.

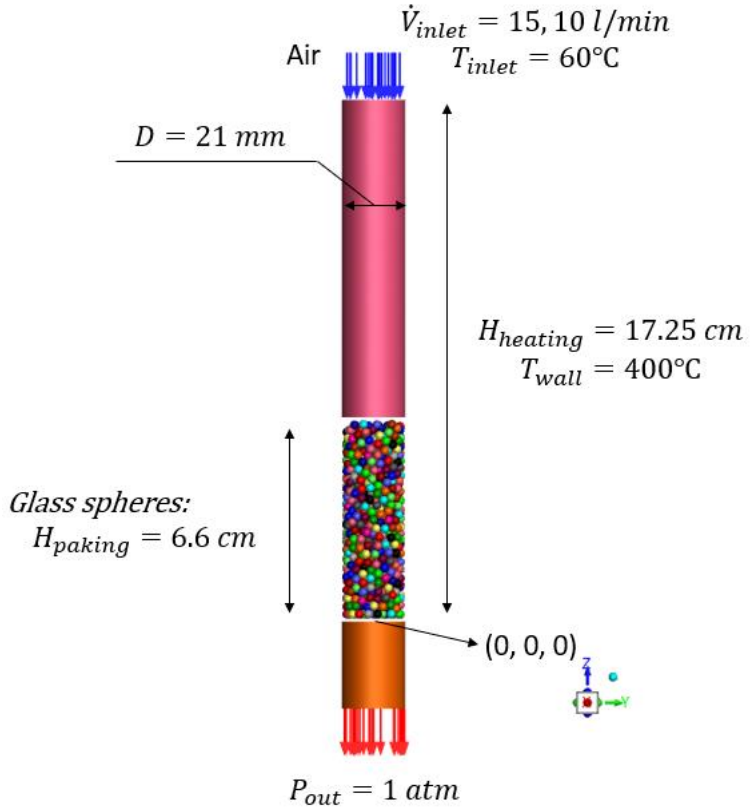

Figure 4-1. Graphic reactor model representation. The wall around the bed has been removed to allow particles appreciation.

Geometrical characteristics

The reactor is a cylinder of *21 mm* inner diameter, the distance between reactor's tube entrance and the end of the bed is of *17.25 cm*. The packed bed is made of glass spherical pellets of *3 mm* diameter and has a height of *6.6 cm*.

Boundary Conditions

The fluid introduced is a gas with characteristics comparable to those of air, at a temperature of *60 °C*. Two volumetric flow inlet velocities were studied in [8], *15 l/min* and *10 l/min*. At the reactor's exit pressure is *1 atm*. The temperature of the reactor's walls is *400 °C* from the inlet to the end of the bed.

Flow Behavior

A comparison between the results considering turbulent and laminar flow is made at [8], concluding that turbulence has nearly no effect on results. This could be consequence of the low flow speeds being the cause of a laminar behavior of the fluid in almost all the volume.
For this reason and in order to decrease computational effort in simulations, turbulent effects have been not considered in the model developed in this thesis.

4.1 PELLETS POSITIONS OBTENTION:

The method the Discrete Element Method (DEM) was chosen to calculate a random arrange of particles inside the reactor. Even though it is the one that more computational effort requires, it is also the one which better simulates the random nature of real packing procedures. The Software used for this task was Blender™.

The procedure followed consisted in letting 1000 spheres of *3 mm* diameter fall inside a cylindrical tube of *21 mm* diameter and *170 mm* heigh, calculating the collisions between them and with the tube wall to determine their final position in the bed.
Was noticed that simulating the 1000 spheres fall at once resulted in too heavy simulations. To reach a stationary state with pellets velocities near to cero was very time consuming and the computational effort required quite high. This was caused due to the large number of collisions happening in every step of the simulation. The solution applied was to divide the 1000 pellets in groups and simulate their fall inside the tube separately, the workflow proceeded as follows.
The 1000 spheres group was divided into 9 groups, 7 of them with 128 spheres each, one of 96 and a last one of 8 spheres. The groups were simulated in that order following the next procedure. A group was simulated calculating its collisions until the pellets reached an almost stationary state, then, their positions inside the tube were fixed. The next group was simulated so its spheres would

fall over the ones of the previous group, however, the collisions between the pellets previously fixed would not be calculated. This made the simulation a lot lighter, and the time required to get a bed geometry much shorter.
During this procedure, was observed that if the first group was generated at great distance to the ground, it was likely for some spheres to go thought the floor. It was also noticed that for great spaces between the groups, some particles would go through the particles previously packed and get trapped inside of the bed. These two events probably happened because of an insufficient number of collisions calculations per time unit. If the space per second travelled by a particle is too high the collision was not calculated, and the particle followed its path without perturbance.
This phenomenon could be avoided by generating the first group at *20 mm* above the ground of the cylinder and generating each group *10 mm* higher than the previous one. As the bed required is 66 mm heigh, the spheres above this value were eliminated.

Another observation was that for insufficient number of frames per second, overlapping between the particles and with the wall took place, the optimum number of frames pers second was found to be 120 fps.

Simulations were made with 10 sub steps per frame and 10 solver iterations, simulations with a greater number of calculations were made and sown to be largely heavier for the same results.

A simulation with 1000 spheres falling at the same time was made to compare the porosity profile of the geometry generated with the one of the groups method, the simulation time was many times bigger and the porosity profiles were very similar.

4.2 CAD GEOMETRY GENERATION

With the *(x, y, z)* positions obtained from the bed generated in Blender™, it was possible to generate a CAD geometry, that could be imported in the CFD software ANSYS®-Fluent. The software used to generate the CAD geometry was ANSYS®-SpaceClaim.

The procedure followed was to generate a solid cylinder with the geometrical characteristics of the pipe around the bed, then generate spheres of *3 mm* diameter in the pellet's positions intersecting with the cylinder and eliminating the volume of the cylinder intersecting with the sphere.

To eliminate the problematic contact points between the particles and with the wall, cuts were made to the spheres when they were generated. The cuts were done where contact points would exist or distance between two surfaces was too small, this was done following the next criterium.

- **Contact points with the wall.**

  A ring with an inner diameter *0.063 mm* smaller than the cylinder was generated, every part of the particles at a distance of *0.063 mm* or less to the wall, therefore intersecting with the ring, was eliminated.

- **Contact points between particles.**

  If the positions of two particles were nearer than *3.03 mm*, a flat cut was made in both particles in a plane normal to the direction of the vector joining the positions, the depth of these cuts was of *0.045 mm*.

Once the fluid surrounding the packed bed had been generated, two more fluid regions were added. One before the packed bed to complete the distance of *17.25 mm* to the inlet. And another one after to avoid recirculation in the fluid behavior at the bed's exit.
As result a geometry with four parts was left, 3 cylinders representing the fluid regions in the reactors and a bulk of spheres used as cut tools representing the pellets.
As the actual spheres are not necessary to define the geometry because the fluid around them already delimitates solid and fluid regions, these were removed from the CAD geometry to avoid problems with the large number of contact points of the spheres with the body representing the fluid which increase the computational effort and are likely to produce errors.

4.3 MESHING

As it has been said in section 3.3.3, a mesh is needed for the main calculation domain. The software used to accomplish this task was ANSYS®-Fluent.
Two polyhedral meshes were generated with different cell sizes for a later study of the meshes characteristics, allowing to determine the one with the most convenient balance between accuracy and computational effort.
The CAD geometry was meshed as a fluid in the 3 cylindrical bodies representing the fluid region. The voids left in the central body when the spheres were eliminated (section 4.2), were identified

as solid regions and meshed in consequence. The boundary conditions between solid and fluid regions were defined as “walls”. Transition layers were added between the phases to correctly consider the effects of the velocity profile near the walls.

4.4 POROSITY CALCULATION AND VALIDATION OF GEOMETRY

At this point a first validation of the geometry can be made by comparing the radial-porosity profile of the bed generated, the void fraction for each radial coordinate, using the data of the DEM simulation and comparing it against the data of the simulation made in [8] and the de Klerk correlation [27]. To generate the porosity profile of the geometry, two methos were used.

In the first method, 100 concentric cylindrical surfaces were generated inside the packed bed, the surface corresponding to fluid regions were integrated and then divided by the total surface integral, giving a value for porosity in that radial coordinate. These values of porosity were the ones utilized to generate the porosity profile inside the bed.

In the second method, a group of points were generated for 100 *radial-coordinates* (r), 200 heights (*z-coordinates*) and 360 *azimuth-coordinates* (θ). The points were compared with the positions of the particles. If the distance between a position and a point was smaller than the radius of the particles, it means that the point is inside the volume occupied by a particle, if the distance was grater, it means the point is in a void region (the region where the fluid would flow) of the bed.
The points were assigned with a value, 0 for solid (inside a particle) and 1 for void (inside the fluid), the number of points outside of the bed for each radial coordinate was divided by the total number of points in that radial coordinate giving the value of porosity for that r. With all these implemented in a python script, the porosity results for a dimensionless value of the bed radius were obtained. The dimensionless radial coordinates were obtained with the equation:

$$\varphi = \frac{(R - r)}{d_p}$$

Equation 4-1. Dimensionless radial coordinate

Being R the radius of the reactor, r the radial coordinate and $d_p$the particle’s diameter.

Porosity Determination Methods Comparison

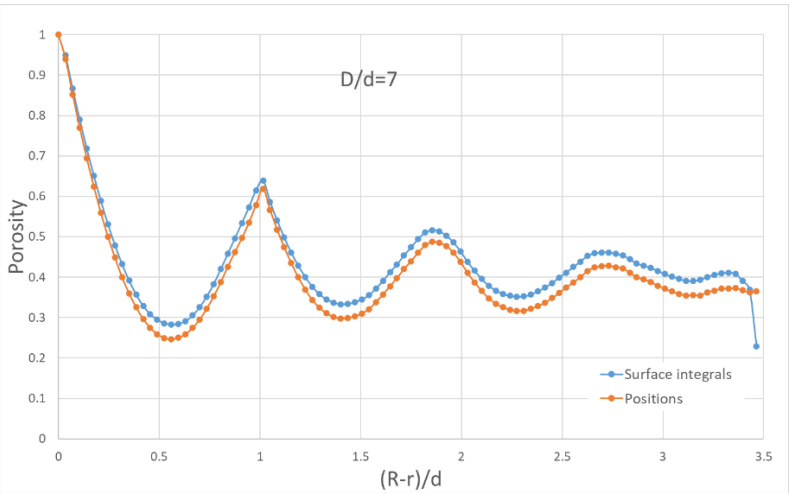

Figure 4-2. Radial porosity profiles obtained with the particles positions of the DEM simulation (Orange) and with the surface integrals in the mesh (Blue).

As can be seen in Figure 4-2, the porosity obtained with the surface integrals method (blue dot-dash line) is slightly higher than the one calculated with the particle's positions (brown dot-dash line). Even so, the two profiles are very similar. That little difference is probably caused by the cuts applied to the particles to avoid contact points; hence less mesh volume is occupied by the pellets slightly increasing porosity.

As in a real particle bed these cuts do not exist, the void profile used for the packed bed validation was the one obtained with the group of points generated inside the bed geometry.

Geometry Validation

The de Klerk correlation is a porosity profile model which divides the packed bed in two regions depending on the *radial-coordinate (r)*, defining the radial values of the porosity using two equations, Equation 4-2 and Equation 4-3, each for a region [27].

$$\varepsilon(r) = 2.14\varphi^2 - 2.53\varphi + 1, \varphi \leq 0.637$$

Equation 4-2. Radial porosity model [27], $\boldsymbol{\varphi \leq 0.637}$

$$\varepsilon(r) = \varepsilon_b + 0.29\exp(-0.6\varphi) * \left[\cos\left(2.3\pi(\varphi - 0.16)\right)\right] + 0.15\exp(-0.9\varphi), \varphi > 0.637$$

Equation 4-3. Radial porosity model [27], $\boldsymbol{\varphi > 0.637}$

Being φ the dimensionless value for the radial coordinate.

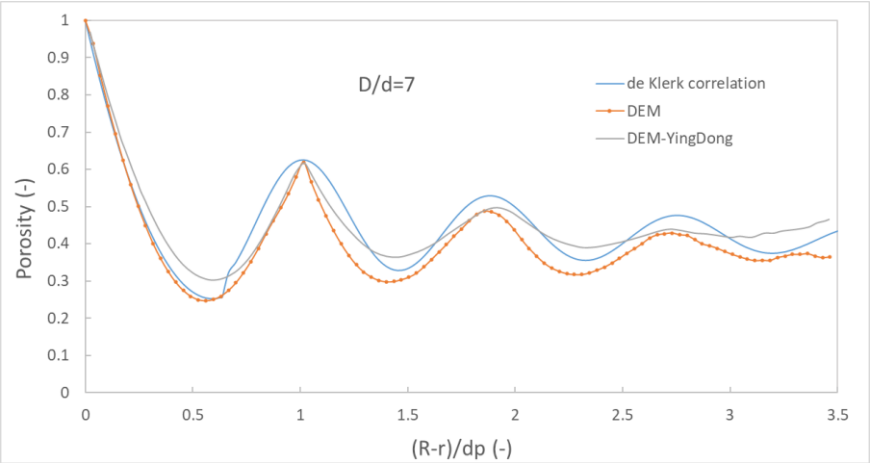

Figure 4-3. Comparison of the radial porosity profile of the DEM generated geometry *D/d=7* obtained in this thesis, the one obtained at [8] and the de Klerk correlation [27].

As can be seen in Figure 4-3, good agreement is found between the porosity profile of the geometry generated with the one from [8] as well as with the de Klerk correlation.

A second DEM geometry with the exact same parameters of the first one was made to ensure that the results were not a coincidence.

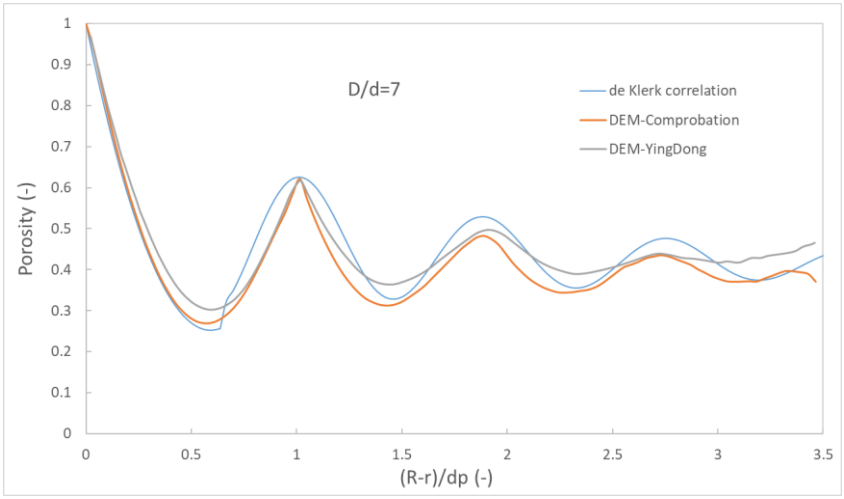

Figure 4-4. Same comparison as the one made at Figure 4-3 but using a different *D/d=7* geometry DEM generated.

As can be appreciated in Figure 4-4, both DEM generated beds have an almost identical porosity profile and both match the reference [8] and the de Klerk correlation. However, the bed geometry could not be contrasted with experimental data as these were not found for *D/d=7* geometries.

In order to validate the method used to generate the bed with experimental data, a last bed of *D/d=5.96*, for which experimental data does exist, was made and compared with the experimental profile available at [28].

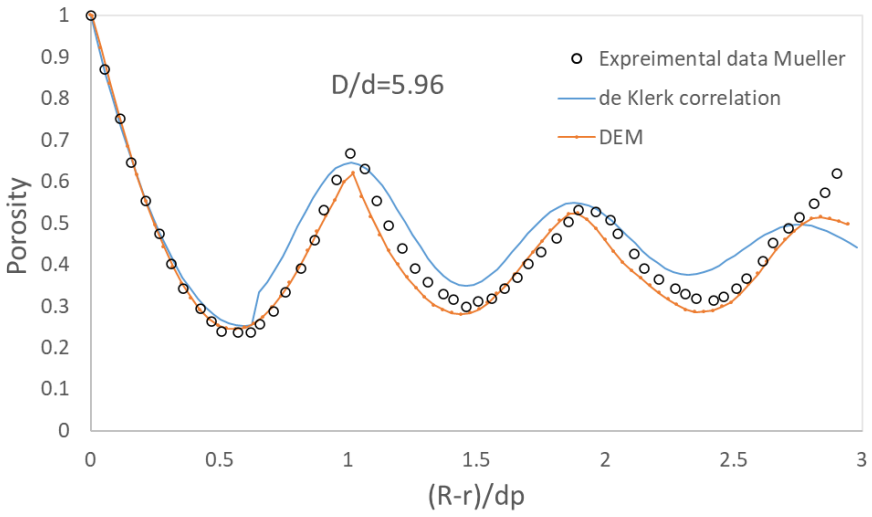

Figure 4-5. Comparison of the porosity profile of a bed geometry of *D/d=5.96* DEM generated with the experimental measures from [28] and with the de Klerk correlation for the mentioned diameter relation.

Figure 4-5 shows the porosity profile of the packed bed with a D/d of *5.96*, with a diameter of *17.88 mm* and the same spherical particles of *3 mm*. This profile is compared with experimental data reported by [28], the DEM simulations made by [8] and the correlation of de Klerk [27]. It sows very good agreement with all of them, so the method used was considered validated as well as the packed beds generated with it.

4.5 FLOW SIMULATIONS

The boundary conditions and material properties, temperature of the walls and the materials properties are the same as the ones used in [8] for this scenario.

As it can be seen at the comparison made in [8], with the low velocities used for this simulation, the Reynold's number has a low value for almost all the flow, so there is nearly no difference between the results obtained the simulations made with the turbulent model and the ones made with laminar model.

4.5.1 Material properties

Air Properties

The air properties relevant for the equations are, density, viscosity, thermal conduction, and specific heat. They all change with temperature and some also does with pressure.

Variations due to pressure in viscosity and density, however, have been neglected in this study. The reason is that pressure changes inside the reactor are relatively small, as can be appreciated in Figure 4-6, and in the case of viscosity, the variation with pressure is very reduced when compared to its variation with temperature Table 1. For density, pressure influence is larger, so a quick study was made to rate its influence in the worst-case scenario.

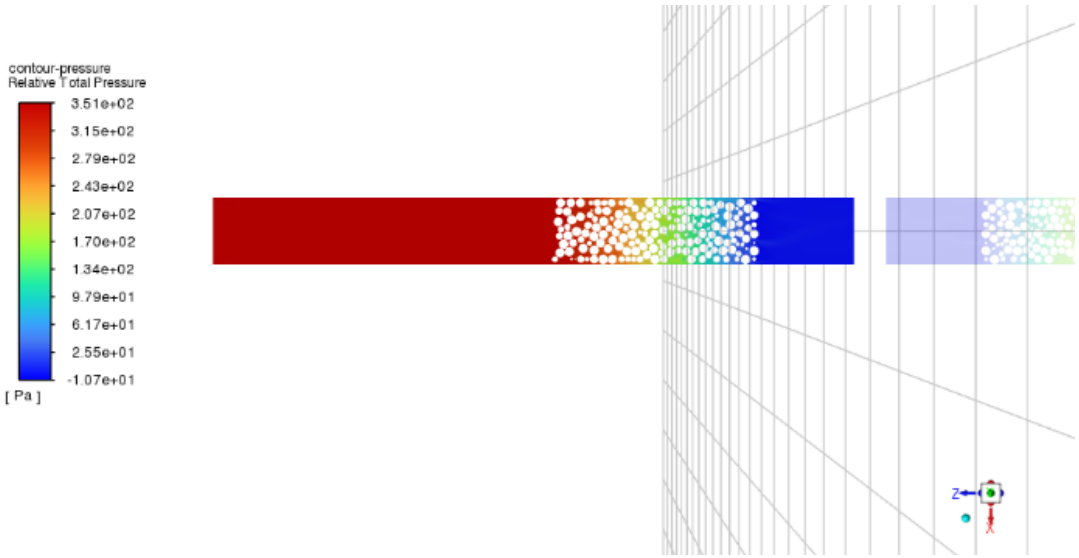

Figure 4-6. Relative pressures inside the CFD solved reactor model.

As it can be appreciated in Figure 4-6, the maximum variation of pressure inside the reactor is of *351 Pa* or *0.00351 bar*. Interpolating at tables for dry air available in [11], the maximum variation of density at *60 °C* is of 5.074×10^{-3} *kg/m*^{3}, a variation of *0.4853%* the value of the density at this temperature. For this change of pressure, the variation of density at *400 °C* is even lower.

However, the variation with the temperature at *1 bar* between *60 °C* and *400 °C* is of *0.5283 kg/m*^{3} or a *50.5308%* its value. The variation of density with the pressure is dismissed in comparison with the variation with the temperature.

Parameter	Variation with pressure
Density (ρ)	With the highest pressure in the reactor 0.4853%
Viscosity (μ)	Increase in 10% each 10 bar [10]
Specific heat (c_p)	No variation with pressure [10]
Thermal conductivity (λ)	No variation with pressure [10]

Table 1. Air's parameters variation with pressure.

The values for density, viscosity, specific heat and thermal conductivity introduced for different values of temperature are taken for dry air at *1 bar* from [11].

Other Materials Properties

Concerning the rest of materials, the only relevant characteristics to the calculations, are density, thermal conductivity, and specific heat, they all have been considered constant.
The materials used for the particles and the walls were taken from the ANSYS®-Fluent material library. Their characteristics can be seen in Table 2.

Part	Material	Porosity (Kg/m^3)	Thermal conductivity (W/(m*K)	Specific heat (J/(Kg*K))
Spherical pellets	Glass-alkali-strontium	2674.9	1.4	748.33
Walls	Aluminum	2719	202.4	871

Table 2. Properties of the solid materials used in the simulation.

4.5.2 Meshes

The first simulation was made with *11 million cells*, but recirculation happened at the exit of the bed, what apparently created a loop trying to resolve the recirculation, also errors happened when data was loaded so the results were discarded as valid.
The densest mesh managed to be generated without recirculation or errors had over *5 million cells*, its generation required great computational effort and time, so a lighter mesh was generated to study the difference in the results obtained with each one.

The lighter mesh had *3079110 cells*, the results for the pressure drop obtained with both meshes are presented at Figure 4-7.

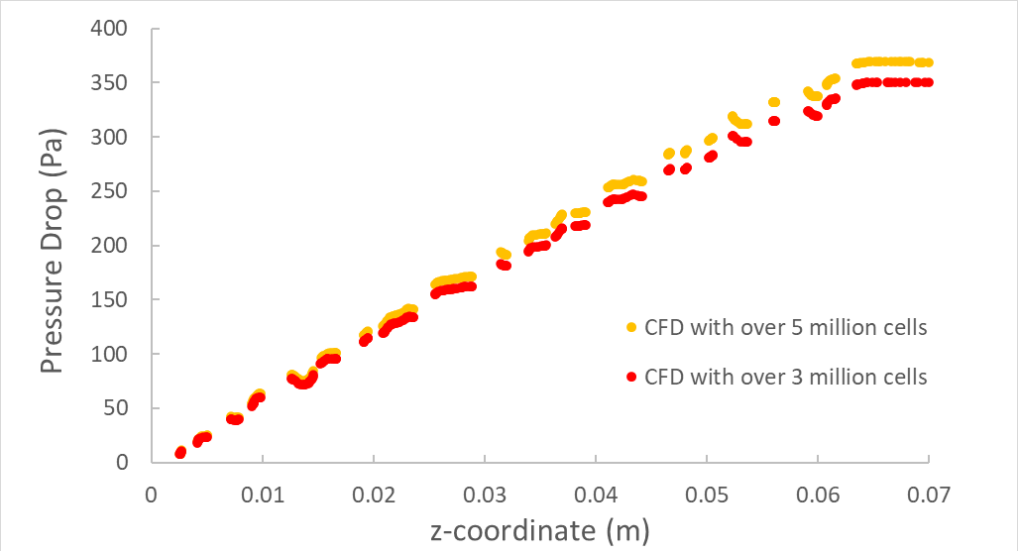

Figure 4-7. Comparison between the pressure drop results for the two meshes generated for a *D/d=7* bed geometry.

As said at section 3.3.3, for a mesh to be valid, the results obtained with it must not variate when compared to the ones obtained with a denser mesh. As can be appreciated at Figure 4-7, the difference between the results obtained with both meshes is almost cero at the beginning of the bed and of around *20 Pa* at the end, however the lighter mesh converged in all the simulations made whereas convergence in the heaviest one was only managed one time. Also, the time difference between both was notable having the heaviest one more than the double of convergence time. For all these reasons, the lighter mesh results were the one used to continue with the model validation dismissing the difference in the results and considering it as sufficiently accurate to the studies wanted to make in this thesis.

4.5.3 Final validation

Once a valid geometry had been obtained and correctly meshed, the results of the CFD simulations were contrasted against the ones simulated and experimentally gotten at [8]. The results available to compare at [8] are the pressure drop along the bed, and the radial distribution of temperature for specific *z-coordinates*.

Pressure drop study.

The relative pressure of the fluid along the bed of particles was measured on a line that crossed the bed through its center, from the top to the bottom. Then these values were represented against the *z-coordinate* where they were measured showing the tendence of pressure drop across the bed as well as the total pressure difference.
The total pressure drop along the bed was also calculated using an empirical model to compare the results.

The empirical prediction was calculated using the Ergun equation, Equation 3-2. The temperature values used to define the viscosity and the density, as well as the superficial velocity were extracted from the CFD simulation for the *z-coordinate = 0.067 m*, just before the beginning of the bed. The measurements of velocity and temperature were made calculating the average value of these fluid parameters in the cross-section area *1 mm* before the bed. The values of density and viscosity were determined for the temperature measured by interpolation of the experimental values from the dry air table available at [11]. All values of variables used in equation can be seen at Table 3 as well as the analytical result.

Just before the bed (z = 0.067)					
Temperature (°C)	Density (Kg/m^3)	Dynamic viscosity (µPa*s)	Superficial velocity (m/s)	Average porosity (-)	ΔL (m)
210.1613	0.7216	26.437	0.9955588	0.408520972	0.066
Total pressure drop (Pa)	387.4460517				

Table 3. Values of the variables used at Equation 3-2 and its result for the total pressure drop along the bed.

To graphically represent the pressure loss across the bed using the result of the Ergun equation, a linear function was defined using the relative pressure at the beginning of the bed (*387.45 Pa* to *z = 0.067 m*) and the relative pressure at the end (considered *0 Pa* at *z = 0 m*).

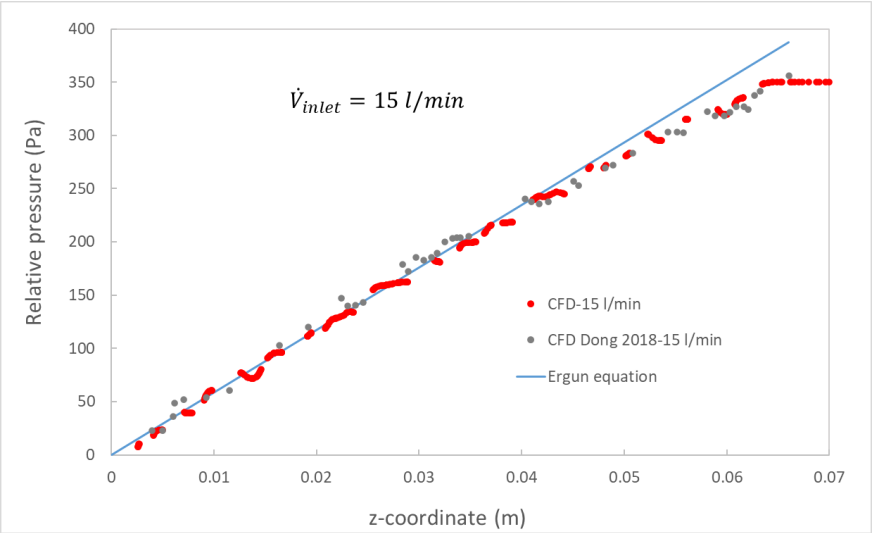

Figure 4-8. Pressure drop results from the CFD simulation compared against the ones obtained from the CFD simulation made in [8] and the Ergun equation. Inlet velocity of the flow of *15 l/min*.

A CFD simulation in the same model was made changing the inlet velocity of the flow from 15 l/min to 10 l/min. CFD simulation data for this velocity is also available at [8]. The Ergun equation was also solved for this scenario in the same way as explained for the previous comparison.

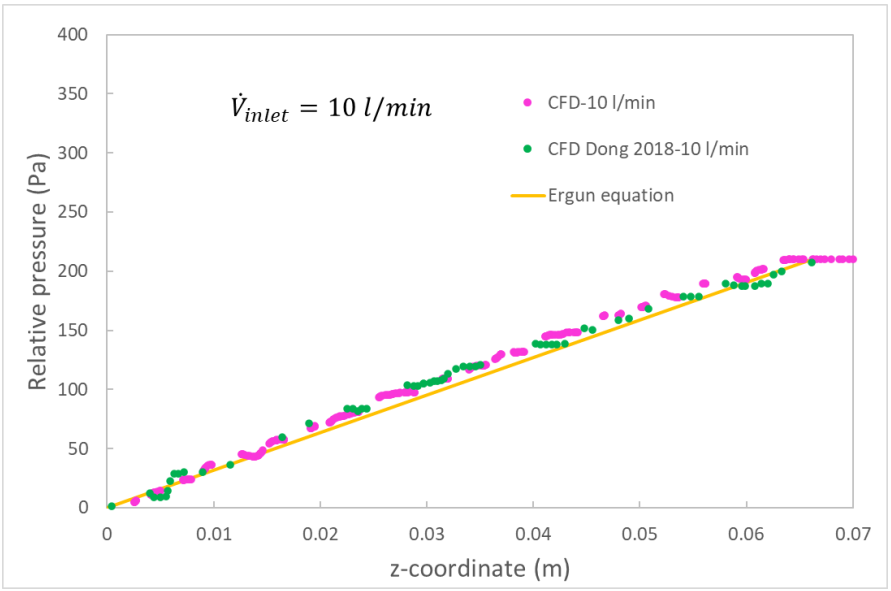

Figure 4-9. Pressure drop results from the CFD simulation compared against the ones obtained from the CFD simulation made in [8] and the Ergun equation. Inlet velocity of the flow of *10 l/min*.

As can be seen at Figure 4-8 and Figure 4-9, the results of the model show very good agreement with the ones from [8]. Also, good agreement is found with the approach made with the Ergun equation.

Radial temperature profile

At the experiment made by [8], a type K thermocouple of *0.5 mm* of diameter was placed across the reactor perpendicular to *z* axe at *z-coordinate = 1.5 mm*, in other to measure the radial temperature profile. Due to the randomly packing process, huge variations were noted when temperatures were measured in a line crossing the reactor in *x* or *y* exes, so in order to obtain more even values, the average temperature was measured for 100 equidistant rings from *x = 0* mm to *x = 105 mm* in a range from *z = 1 mm* to *z = 2 mm*. Each average value is represented for its *radial-coordinate (r)* at Figure 4-10.

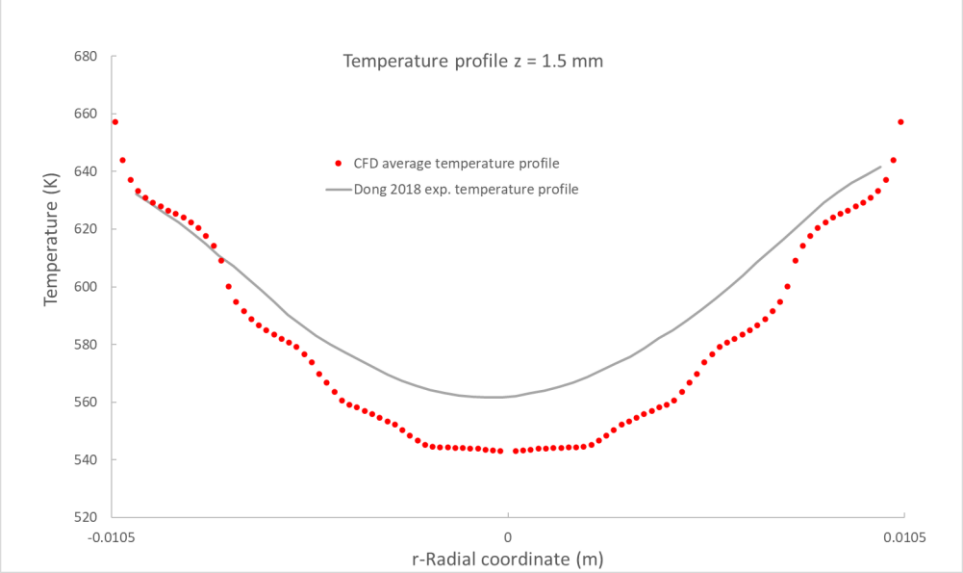

Figure 4-10. Radial temperature distribution at *z = 1.5 mm* calculated ta the CFD simulation compared against the experimental data from [8]. The average temperature is calculated in a range of *1 mm* between *z = 1 mm* and *z = 2 mm*.

In Figure 4-10 can be appreciated a really good correlation of the experimental values from [8] (gray line) with the ones of our model (red dots-line). The correlation with experimental data is not as good at the center as at the extremes, with a difference of approximately of *20 K*, but still close.

Conclusion

In view of the good agreement found between the theorical and experimental data from the references [8] and [28], this chapter provides validation of the DEM-CFD model designed as well as well as of the methods used to generate it. The approaches of heat transfer and pressure drop made solving this model will be considered valid for different comparisons in section 5.

5 RESULTS

5.1 CONTACT POINTS.

The method used in Dong 2018 [8] to avoid contact points is different from the one used in this thesis, so some assumptions can be made by comparison of the final results.

The contact points of the geometry used in [8] are eliminated using a complex algorithm which deforms the mesh. This algorithm increases the distance between the particles by decreasing the size of the meshed particle cells in function of the proximity with other cells of the same type, increasing the width of the fluid cells between them as can be seen at Figure 5-1. Local flattening of cells for reduced sizes of the volume to mesh [8]., creating a smooth progressive flattering where contact points are and leaving a wither space between them occupied by fluid cells.

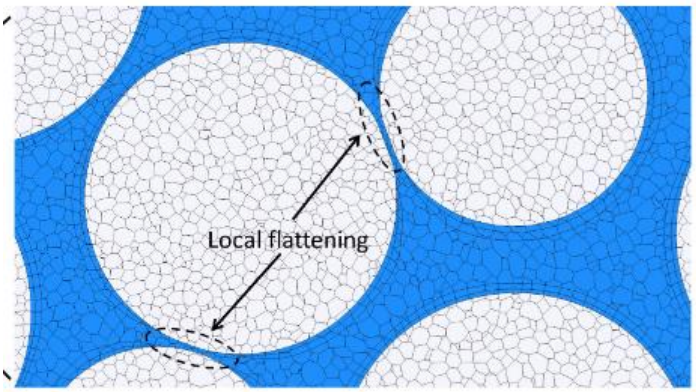

Figure 5-1. Local flattening of cells for reduced sizes of the volume to mesh [8].

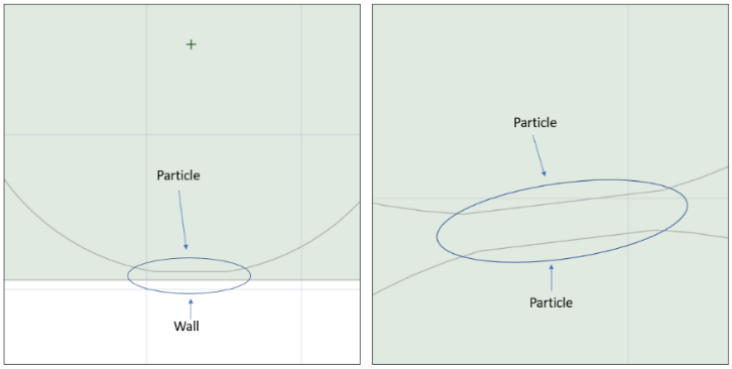

Figure 5-2. Elimination of contact points by flat cuts in the particles.

However, in the geometry design in this thesis, the contact points have been eliminated by making a flat cut in the particles and creating two flat surfaces, one in front of the other, where the contact point was, as is explained at section 4.2.. The result can be seen at Figure 5-2.

The method used in this thesis is implemented by a simpler algorithm, however the resulting changes on pellets surfaces is less progressive. Even so, as can be appreciated in Figure 4-8 and Figure 4-9, the results for the pressure drop along the bed are practically the same, so an assumption can be made that, at least for the pressure drop, the differences between these two methods of contact points elimination makes not notable difference.

5.2 TEMPERATURE PROFILE

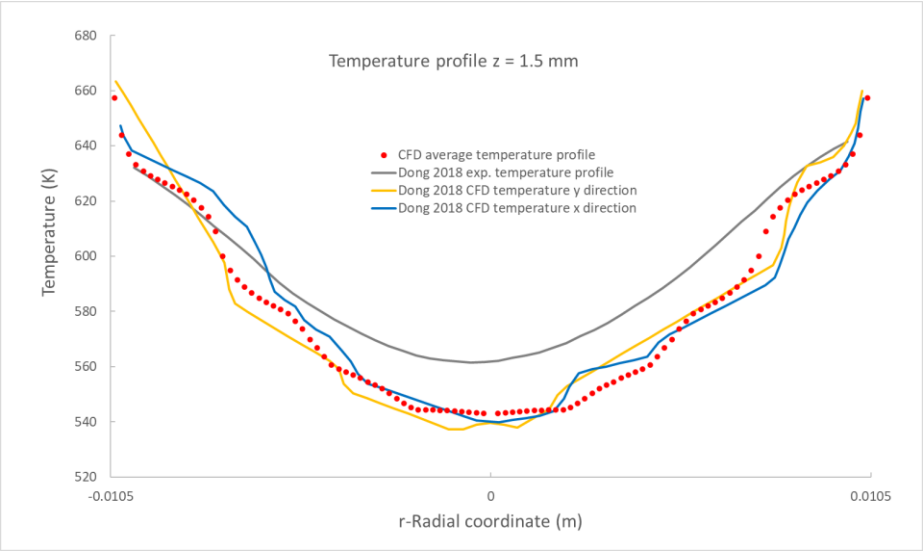

Figure 5-3. Comparison of the temperature profile results gotten in the CFD simulation against the experimental and simulated data taken from [8] at *z = 1.5mm*.

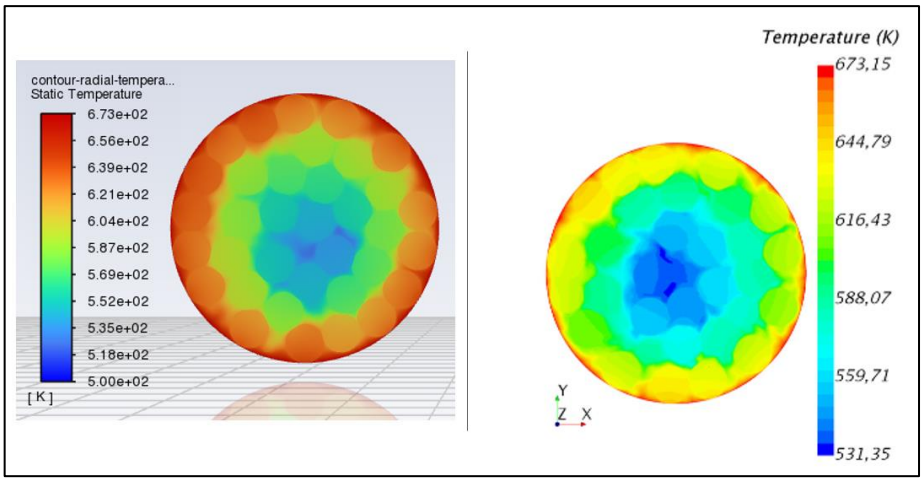

Figure 5-4. Radial temperature fields in *z=1.5 mm* for a flux of *15 l/min*. the one of the left is the result of the CFD simulation of the model generated in section 4, the one of the right is from the CFD done in [8].

Comparing the temperature profile results with the ones from the CFD simulation made at [8] difference in the continuity of the curve can be appreciated (see at Figure 5-3), this happens because a different method is used to make the measurement. At [8] temperature values are measured at the axes *x* and *y*, whereas the method followed in this thesis was to calculate the average value for each *radial coordinate* (r). The discontinuity in the slope of the curve is due to the heterogeneous axial void factor what makes that the axes that the exes intersect with different amount of solid phase belonging to the particles. For that reason, an average temperature of the fluid phase has been considered a more realistic option, and as can be seen at Figure 5-3, the curve shape is more similar to the experimental, with less temperature jumps than the measurements done in the axes.

5.3 ERGUN EQUATION

Equation 3-2 has been used at used at section 4.5.3 to compare it with the CFD simulation results, the value obtained for the total pressure is pretty close to the total pressure drop measured in the simulation. The decrease in relative pressure along the bed has an almost linear behavior, what makes the linear approach, although not perfect, quite accurate in every *z-coordinate*.

In the case where the inlet velocity is of *15 l/min* (Figure 4-8), the difference between the total pressure drops predicted by each method is of about *30 Pa*, being the calculated with the Ergun equation of *387.45 Pa* and the CFD calculated of *350 Pa*.

Maximum difference between the curves happens to be at the beginning of the bed, where the slope is softer in the CFD results.

In the case where the inlet velocity is of *10 l/min* (Figure 4-9), both approaches show very god correlation, however, in this case the total pressure drop is practically the same, but as a consequence of the smaller slope at the beginning, the rest of the curves do not match as well as in the previous case.

However, this good approach with the empirical correlation has been managed thanks to the average data of velocity and temperature at the inlet of the bed. No other way of getting these results with the Ergun equation has been found.
Not so good approaches were achieved for other CFD simulations with all the fluid flow at the same temperature with no heat transference, where the temperature and velocity at the inlet of the bed are almost the same as at the inlet of the reactor's tube so they are known before the simulation. (The generation of this model is explained at 5.4)

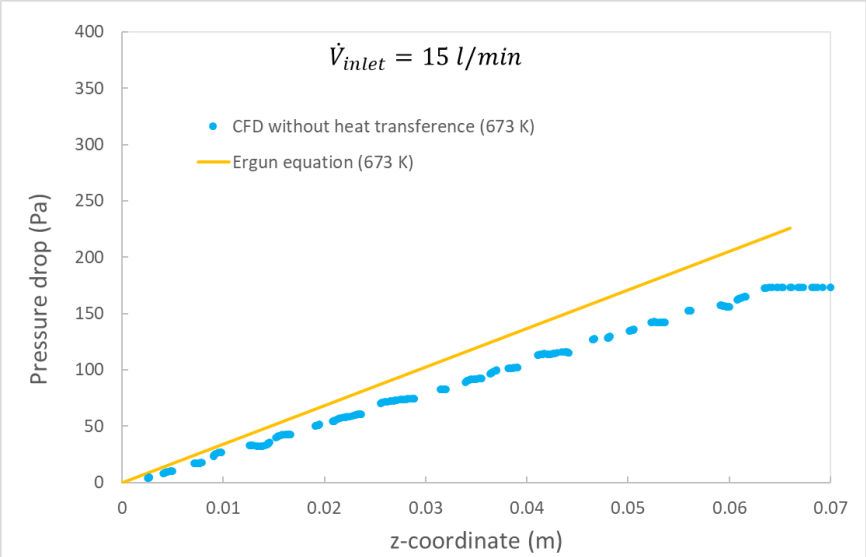

Figure 5-5. Comparison of the pressure drop measured from the data of a CFD simulation against the calculated with the Ergun equation. The temperature of the fluid was *673 K* in all the volume, heat transference was neglected, and the flow velocity was set at the inlet at *15 l/min*.

At Figure 5-5 can be seen as the Ergun equation provides a worse approach, the difference of the total pressure drop in this case is about *50 Pa*.

The different behavior of the Ergun equation in the cases shown, is probably because it neglects the local effects as well as the heat transfer. What leads to think that the better correlation with the CFD simulations where heat transference has been considered is just a coincidence. The numerous variables that affect the result, density, viscosity, and velocity, make that, with the simulations and study made in this thesis, no assumptions can be done for the behavior of this empirical correlation with different flow conditions for the same reactor.

Would be interesting trying to achieve realistic values for the temperature and the velocity before the bed with a porous medium model, which requires much less computational effort (section 3.3.1), for use them on the Ergun equation. Would make the study faster.

5.4 SIMULATIONS WITHOUT THE ENERGY EQUATION

For this first study, the objective was to determine the influence in the pressure drop of the heat transference in a heated fixed bed reactor. The procedure followed was to compare the results of simulations where the Energy Equation (Equation 3-15) against simulations considering it.

Model without heat transfer

For the study of this model, the interior of the particles does not need to be considered, as the interaction will always take place on their surfaces. So, a new mesh was generated using the same CAD geometry as used in the validation section 4.2.. This new mesh with void pellets had *1924173 cells*, much lighter than the one made for the validated model.
The air properties were defined as constant values as temperature will not change and the pressure variation is neglected, so them were taken from the dry air at 1 atm tables from [11] for the temperature required in the simulation. The rest of parameters were set as in the validated model.

Model with heat transfer

The results for a heat transfer model were taken from the model generated and validated in section 4.

Results

A uniform temperature of *400 °C* was considered for all the fluid volume at the model without heat transference, the convergence of calculations was, as expected, much faster than for the validated model as the number of calculations and cells were significantly lower. The result of the pressure drop along the bed is shown below.

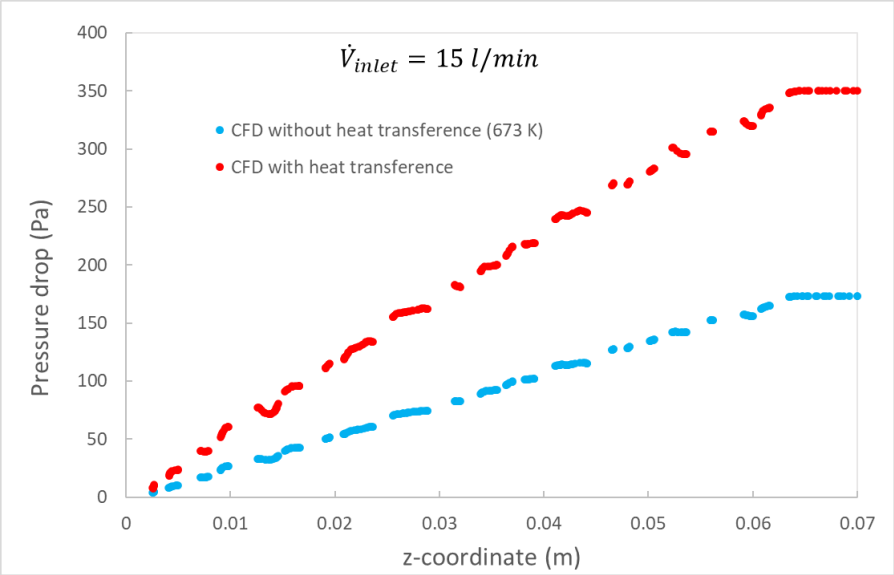

Figure 5-6. CFD pressure drop results with and without applying the energy equation. Flux velocity of *15 l/min*.

As can be seen at Figure 5-6, pressure drop considerably decreases when energy equation is neglected, and all the fluid is at *400 °C*. A change in the results is logical as variations in density and viscosity with temperature were not considered.

A significant increase of *z* velocity was noticed just before the bed in the heated model, while this phenomenon did not take place in the one with constant flow temperature.

This effect was consequence of the progressive heating of the fluid, an increase in the fluid temperature causes a decrease in in its density, by mass conservation, means an increase in its volume, what progressively pushes the fluid resulting in a continuous velocity rise as it is heated up. The two forces standing against the fluid advance and causing the pressure drop are viscous loss resistance and inertia loss resistance [7], and both are directly proportional to the velocity so a rise in velocity would be traduced in a rise in pressure drop.

The model was solved for a temperature of *100 °C* (greater densities), also for a velocity inlet of *15 l/min* and the pressure drop was slightly different than for *400 °C* (greater viscosities), but still a lot lower than with the principal model, however, great changes were noticed for different velocities. So, an assumption could be made that the principal factor o the huge difference between the models results, is the velocity variation due to the density changes.

6 CONCLUSIONS AND PROSPECTIVE STUDIES

6.1 EMPIRICAL CORRELATIONS

As said in section 5.3, would be interesting trying to achieve realistic values for the temperature and the velocity using a lighter porous medium model to calculate realistic values for the temperature and velocity of the flow before entering in the packed bed. This could be an accurate and fast method to calculate empirical correlations to use in empirical models, like the Ergun equation, for a wide range of specific cases.

6.2 POROUS MEDIUM MODEL

Fluent model the porous media by adding a momentum source term to the fluid flow equations. This source term is composed by the viscous loss (first term on the right side of Equation 6-1), given by the Darcy equation (Equation 3-3), and the inertial loss (second term on the right side of Equation 6-2) [29].

$$S_i = -\left(\sum_{j=1}^{3} D_{ij}\mu v_j + \sum_{j=1}^{3} C_{ij}\frac{1}{2}\rho|v|v_j\right)$$

Equation 6-1. Momentum source term.

Being S_i the source term for an i momentum equation in the (x, y, z) space, $|v|$ is the magnitude of the velocity and D and C are prescribed matrices. This momentum creates a pressure drop proportional to the fluid velocity in the cell.

Fluent allows to model the source term velocity power law given by the following expression [29]:

$$S_i = -C_0|v|^{C_1} = -C_0|v|^{(C_1-1)}v_i$$

Equation 6-2. Source term power law.

Where C_0 and C_1 are user-defined empirical coefficients. These empirical coefficients can be determined for a certain type of reactors by the PRCFD method, in a way that can be used in PMM models for a range of different reactors with similar geometrical characteristics. This would allow to get accurate results without creating a particle bed geometry and with much lighter simulations (section 3.3.1).

To generate a library of these empirical coefficients, a possible procedure would be to determine the coefficients for a specific reactor using the results of a PRCFD approach. Then determine the range where those coefficients still providing accurate results while variating geometrical characteristics like the reactor or pellets diameter or le bed length. The same study could be done changing the velocity of the flow. Evolution with temperature for different heated reactors would be an also interesting study.

6.3 CONCLUSIONS

PRCFD models are quite accurate tools to approach the flow and heat transfer behavior in fixed bed reactors. However, the laborious task of modelling a detailed geometry and the high computational cost of the simulations, are limiting factors that hinder their application, especially in regular computer hardware such as the one used for this thesis. For this reason, a very interesting application of this models, is the determination of empirical correlations, which can be implemented in simpler models of common use in order to improve their accuracy.

The combination of PRCFD and PMM models is a promising alternative to traditional empirical methods. The use of empirical correlations determined by PRCFD in PMM models would lead to more accurate and realistic approaches with more affordable simulations from a hardware point of view. For this to be a viable option, libraries of empirical correlations must be created, and the range of usability of each must be determined for reactors with different characteristics.

7 BIBLIOGRAPHY

[1] H. Ritchie, M. Roser, y P. Rosado, «Energy», Publ. Online OurWorldInDataorg, 2022, [Online]. Disponible en: 'https://ourworldindata.org/energy' [Online Resource]

[2] IEA (2022), Global Hydrogen Review 2022, IEA, Paris https://www.iea.org/reports/global-hydrogen-review-2022, License: CC BY 4.0

[3] Worldometers.info (2023) Oil reserves by country, Worldometer. Worldometers.info. Available at: https://www.worldometers.info/oil/oil-reserves-by-country/ (Accessed: February 20, 2023).

[4] Stocker, T.F.; Qin, D.; Plattner, G.-K.; Tignor, M.; Allen, S.K.; Boschung, J.; Nauels, A.; Xia, Y.; Bex, V.; Midgley, P.M. IPCC, 2013: Summary for Policymakers. In Climate Change 2013: The Physical Science Basis. Contribution of Working Group I to the Fifth Assessment Report of the Intergovernmental Panel on Climate Change; Cambridge University Press: Cambridge, UK; New York, NY, USA, 2013.

[5] E. Rivard, M. Trudeau, y K. Zaghib, «Hydrogen Storage for Mobility: A Review», Materials, vol. 12, n.o 12, p. 1973, jun. 2019, doi: 10.3390/ma12121973.

[6] Union Of Concerned Scientists. (2014) Union of Concerned Scientists UCS. United States. «How-Clean-Are-Hydrogen-Fuel-Cells-Fact-Sheet.pdf» Retrieved from, https://www.ucsusa.org/resources/how-clean-are-hydrogen-fuel-cell-vehicles.

[7] A. G. Dixon y B. Partopour, «Computational Fluid Dynamics for Fixed Bed Reactor Design», Annu. Rev. Chem. Biomol. Eng., vol. 11, n.o 1, pp. 109-130, 2020, doi: 10.1146/annurev-chembioeng-092319-075328.

[8] Y. Dong, «Modeling chemistry and flow in catalytic fixed-bed reactors with detailed geometry», TUHH Universitätsbibliothek, 2018. doi: 10.15480/882.1636.

[9] N. Jurtz, M. Kraume, y G. D. Wehinger, «Advances in fixed-bed reactor modeling using particle-resolved computational fluid dynamics (CFD)», Rev. Chem. Eng., vol. 35, n.o 2, pp. 139-190, feb. 2019, doi: 10.1515/revce-2017-0059.

[10] F. M. White, "Fluid Mechanics," 7th Edition, McGraw- Hill, New York, 2011.

[11] VDI e. V., Ed., VDI Heat Atlas. Berlin, Heidelberg: Springer Berlin Heidelberg, 2010. doi: 10.1007/978-3-540-77877-6.

[12] C. Y. Wu, Y. M. Ferng, C. C. Chieng, y C. C. Liu, «Investigating the advantages and disadvantages of realistic approach and porous approach for closely packed pebbles in CFD simulation», Nucl. Eng. Des., vol. 240, n.o 5, pp. 1151-1159, may 2010, doi: 10.1016/j.nucengdes.2010.01.015.

[13] Ansys® Fluent, Release 2023 R1, help system, Ansys Fluent Theory Guide, ASYS, Inc.

[14] «Maestri M, Cuoci A. 2013. Coupling CFD with detailed microkinetic modeling in heterogeneous catalysis. Chem. Eng. Sci. 96:106–17».

[15] A. Züttel, «Materials for hydrogen storage», Mater. Today, vol. 6, n.o 9, pp. 24-33, sep. 2003, doi: 10.1016/S1369-7021(03)00922-2.

[16] S. Sharma, S. Agarwal, y A. Jain, «Significance of Hydrogen as Economic and Environmentally Friendly Fuel», Energies, vol. 14, n.o 21, p. 7389, nov. 2021, doi: 10.3390/en14217389.

[17] P. Sterchele et al., «The German energy transformation in its social context».

[18] A. Ariharan, B. Viswanathan, y V. Nandhakumar, «Nitrogen-incorporated carbon nanotube derived from polystyrene and polypyrrole as hydrogen storage material», Int. J. Hydrog. Energy, vol. 43, n.o 10, pp. 5077-5088, mar. 2018, doi: 10.1016/j.ijhydene.2018.01.110.

[19] E. Masika y R. Mokaya, «Preparation of ultrahigh surface area porous carbons templated using zeolite 13X for enhanced hydrogen storage», Prog. Nat. Sci. Mater. Int., vol. 23, n.o 3, pp. 308-316, jun. 2013, doi: 10.1016/j.pnsc.2013.04.007.

[20] M. S. Yahya y M. Ismail, «Synergistic catalytic effect of SrTiO3 and Ni on the hydrogen storage properties of MgH2», Int. J. Hydrog. Energy, vol. 43, n.o 12, pp. 6244-6255, mar. 2018, doi: 10.1016/j.ijhydene.2018.02.028.

[21] B. Bogdanović, M. Felderhoff, A. Pommerin, F. Schüth, y N. Spielkamp, «Advanced Hydrogen-Storage Materials Based on Sc-, Ce-, and Pr-Doped NaAlH4», Adv. Mater., vol. 18, n.o 9, pp. 1198-1201, may 2006, doi: 10.1002/adma.200501367.

[22] Spreitzer D, Schenk J. Reduction of iron oxides with hydrogen—a review. Steel Res Int 2019;90:1900108. https://doi.org/10.1002/srin.201900108.

[23] M. B. Ley et al., «Complex hydrides for hydrogen storage – new perspectives», Mater. Today, vol. 17, n.o 3, pp. 122-128, abr. 2014, doi: 10.1016/j.mattod.2014.02.013.

[24] L. Morris et al., «A manganese hydride molecular sieve for practical hydrogen storage under ambient conditions», Energy Environ. Sci., vol. 12, n.o 5, pp. 1580-1591, 2019, doi: 10.1039/C8EE02499E.

[25] «Betsch, K.; Knauf, G.; Kobow, C.; Martin, H.; Petzold, D.; Ufer, J.; Wolf, B. Verfahren zur Erzeugung von Wasserstoff oder wasserstoffreichen Gasen, 1972. DD 000,000,094,984, 1 March 1972.».

[26] L. Brinkman, B. Bulfin, y A. Steinfeld, «Thermochemical Hydrogen Storage via the Reversible Reduction and Oxidation of Metal Oxides», Energy Fuels, vol. 35, n.o 22, pp. 18756-18767, nov. 2021, doi: 10.1021/acs.energyfuels.1c02615.

[27] A. de Klerk, «Voidage variation in packed beds at small column to particle diameter ratio», AIChE J., vol. 49, n.o 8, pp. 2022-2029, 2003, doi: 10.1002/aic.690490812.

[28] G. Mueller, «Numerically packing spheres in cylinders», Powder Technol., vol. 159, pp. 105-110, nov. 2005, doi: 10.1016/j.powtec.2005.06.002.

[29] Ansys® Fluent, Ansys® Fluent, Release 2022 R2, help system, Ansys Fluent User's Guide, ASYS, Inc., help system, Ansys Fluent Theory Guide, ASYS, Inc.

FIGURES INDEX

TABLES INDEX

EQUATIONS INDEX

SYMBOL AND ABBREVIATION DIRECTORIES

Symbol directory

Symbol	Meaning	Units
P	Pressure	Pa
T	temperature	K
$D\|d$	Diameter	m
$R\|r$	Radius	m
D/d	Diameter ratio	(-)
V	Volume	m^3
ε	Porosity / void fraction	(-)
η	Dynamic viscosity	kg/m s
v	Superficial velocity	m/s
L	Length	m
ρ	Density	Kg/m^3
$\dot{V}$	Volumetric flow	l/min
H	Heigh	m
φ	Dimensionless radial coordinate	(-)
c_p	Specific heat at constant pressure	J/(kg K)
c_v	Specific heat at constant volume	J/(kg K)
λ	Thermal conductivity	W/(m K)
t	Time	s
$\vec{v}$	Velocity vector	m/s
h	Enthalpy	J/mol
e	Gravimetric density	wt%
U	Volumetric energy density	MJ/l

Abbreviation directory

IEA	International Energy Agency
CFD	Computational Fluid Dynamics
DEM	Discrete Element Method
PRCFD	Particle Resolved Computational Fluid Dynamics
PMM	Porous Medium Model
FV	Finite Volume
FE	Finite Element

EIDESSTATTLICHE ERKLÄRUNG

Hiermit versichere ich, Ángel Valle Gaisán, die vorliegende Arbeit selbständig, ohne fremde Hilfe und ohne Benutzung anderer als der von mir angegebenen Quellen angefertigt zu haben. Alle aus fremden Quellen direkt oder indirekt übernommenen Gedanken sind als solche gekennzeichnet. Die Arbeit wurde noch keiner Prüfungsbehörde in gleicher oder ähnlicher Form vorgelegt.

Dresden, 2023-02-28

VALLE GAISAN ANGEL - 71188047B

Firmado digitalmente por VALLE GAISAN ANGEL - 71188047B
Fecha: 2023.06.14 19:32:39 +02'00'

Ángel Valle Gaisán